UNIVERSIDAD NACIONAL AUTÓNOMA DE MÉXICO

PROGRAMA DE MAESTRÍA Y DOCTORADO EN INGENIERÍA
ENERGÍA – SISTEMAS ENERGÉTICOS

DEVELOPMENT AND CHARACTERIZATION OF REUSABLE ACTIVATED CARBON FROM MACADAMIA NUT SHELL FOR AMOXICILLIN AND METHYLENE BLUE DYE ADSORPTION

TESIS
QUE PARA OPTAR POR EL GRADO DE:
MAESTRA EN INGENIERÍA

PRESENTA:
ESTEFANIA DUQUE BRITO

TUTOR PRINCIPAL
DR. UGOCHUKWU PATRICK OKOYE
INSTITUTO DE ENERGÍAS RENOVABLES, UNAM

MÉXICO, CIUDAD DE MÉXICO SEPTIEMBRE 2023

JURADO ASIGNADO:

Presidente: Dra. Heidi Isabel Villafán Vidales

Secretario: Dra. Dulce María Arias Lizárraga

1er vocal: Dr. Ugochukwu Patrick Okoye

2do vocal: Dra. Adriana Margarita Longoria Hernández

3er vocal: Dr. Alejandro Ayala Cortés

Lugar donde se realizó la tesis:

Instituto de Energías Renovables, UNAM
Temixco, Morelos

TUTOR DE TESIS:

DRA. UGOCHUKWU PATRICK OKOYE

INSTITUTO DE ENERGÍAS RENOVABLES, UNAM

_____

FIRMA

Abstract

Currently, one of the main damages caused to the environment is related to the uncontrolled disposal of chemical products into bodies of water, causing harmful effects on aquatic life and human health. Some examples of these substances are dyes, pharmaceuticals, metal ions (arsenic, lead, etc.), and pesticides; all of which are difficult to break down and are toxic in high concentrations. In response to this problem, this work developed and characterized macadamia nutshell-based activated carbon for the removal of amoxicillin and methylene blue from a binary solution in an aqueous system.

On the one hand, amoxicillin is an antibiotic used to treat bacterial infections and on the other hand, methylene blue is a cationic dye widely used in the textile industry. Both contaminants are already present in water effluents and in high concentrations could be dangerous to maintain a healthy life. This mixture may give an approach to the adsorption processes in a real context to treat wastewater that is composed of multiple components of different nature.

In this sense, activated carbons were produced through a Box Behnken experimental design, using macadamia nutshell as precursor. Different conditions of activation temperature, time, and potassium carbonate (K_2CO_3): precursor ratio were proved. The resulting activated carbon was employed in binary adsorption process to remove cationic methylene blue dye, and anionic molecule of amoxicillin. The experimental conditions tested varying the pH (2 - 12), initial concentration of binary solution (50, 100, 200, 400, 600 and 800 mg/L, relation 1:1 between both pollutants), adsorbent dosage (0.1-0.3 g), temperature (30, 40 and 50 °C), and time (0-24 h).

The activation conditions tailored topology, functional groups, and morphology of the activated carbon. It was found that the optimum activation conditions were 900 °C, for 1 h and K_2CO_3: precursor ratio of 2:1 (Run 2). This sample shows an appreciably high surface area BET of 1225 m^2/g, pore volume of 0.81 m^3/g, and a nanopore size of 0.46 nm.

The results of binary adsorption revealed that the Run 2 could reach a maximum experimental adsorption capacity of 788.305 mg/g, having better affinity to adsorb the methylene blue contaminant. Evaluated isotherm models demonstrates that Khan isotherm best describes the affinity of the binary solution to Run 2. The pseudo-order second kinetic model best describes the data, which means that the adsorption mechanism was purely chemisorption. The interparticle diffusion test revealed that the adsorbent produced fast adsorption behavior at the initial process; additionally, these

results mostly showed two stages of adsorption.

Likewise, four activated carbon regeneration methods were tested, being the one elaborated with ethanol and sodium hydroxide the one that showed the best performance throughout the regeneration cycles to which it was subjected. However, most of the textural properties of the original activated carbon sample were modified.

Acknowledgement

To each person involved in this thesis work and who made it possible, thanks for the academic and technical support and effort that made this project possible.

To Consejo Nacional de Humanidades, Ciencia y Tecnología (CONAHCyT), for the scholarship that was awarded to me and made it possible for me to pursue my master's studies.

To Univeridad Nacional Autónoma de México (UNAM) and Instituto de Energías Renovables (IER) for once again giving me the privilege of belonging to this beautiful community and giving me the opportunity to learn from experts.

To the projects from Dirección General de Asuntos del Personal Académico, México bajo Programa de Apoyo a Proyectos de Investigación e Innovación Tecnológica (DGAPA-PAPIIT) Project Nos: IA102522, y IG100217 and to Dirección General de Asuntos del Personal Académico, México bajo Programa de Apoyo a Proyectos para lnnovar y Mejorar la Educación (PAPIME) Project Nos: PE104123, which provided the necessary financing for reagents and materials needed to develop this thesis project.

I thank to Dr. Patrick Ugochukwu Okoye, for being my advisor throughout my master's studies and for the corrections made whenever the project required it.

To Dr. Adriana Margarita Longoria Hernández, for the learning provided since my undergraduate studies until now. To Dr. Alejandro Ayala Cortés for his contributions and comments on this work, as well as for the years of friendship, support, and always good cheer.

To Dr. Dulce María Arias for her guidance and recommendations for this work, and likewise to Dr. Heidi Isabel Villafán Vidales for the support in my training as a student and for the comments made for this document.

In particular, I thank Dr. Rocío Nava Lara for providing the resources to carry out the FTIR analysis; likewise, to Ing. Rogelio Morán Elvira for helping with the SEM and EDS analysis.

Particularly, I thank my mother, Guillermina Brito Osorio, who was with me at every step, encouraging me and, above all, giving me all the love and support I needed to get ahead. The words are not enough for me to express what I really feel, but I know that

in our hearts and in our souls, we know and understand better. To my father, José Duque Duarte, for teaching me the path to professional growth with his example.

I also thank Javier Cisneros Brito for his support, even from a distance and in any circumstance. Karla Duque Brito, because, thanks to her maturity, she has taught me to be a better human being. Gael Xavier Cisneros Prado, who brings more joy and light into my life every time I see him. To María Santos Osorio Ramírez for her affection and tenderness that characterize her.

Likewise, I would like to express my gratitude to the friends that I made throughout my stay in this institution and who made my days lighter and more enjoyable. Among them are Sergio Fernando Rodriguez Contreras, Diego Ramón Lobato Peralta and especially Yazmín Karin Ortiz Olivares, for always watching over me and for her sincerity and unconditional support at important moments.

Finally, I would like to dedicate several lines to thank me. For doing this hard work, to overcome the screams, the discouragements and obstacles appeared along the way. For all those days, when I was not mentally well and still did the corresponding work. And above all, for not paying attention to those voices (external and internal) that said that this was not a job for someone like me.

Contents

List of Figures

List of Tables

Chapter 1

Introduction

The earth has been subject to numerous changes and natural phenomena necessary to maintain safe life, however, in the last few years, this dynamics have been disrupted due to environmental problems and other factors. Anthropogenic activities, increasing population growth and increasing industrialization are the primary factors that have disturbed the earth environmental balance. The damages inflicted due to excessive use and discharge of uncontrolled chemical substances (1) affects the aqua bodies, which have an adverse effects on aquatic life and humans (2).

The Guidelines for Quality Drinking-Water published in 2022 by the World Health Organization indicated that the common illnesses caused by consuming or being in contact with polluted water are diarrhoea, cholera, hemolytic uremic syndrome, cancer, hepatitis, and gastroenteritis, among others (3). According to the World Health Statistics 2022 published by the same institution, more than a quarter of the global population had problems accessing safely managed drinking water services in 2020, i.e. about two billion people. Furthermore, only 54% of the global population has access to good sanitation services, which means that the water used by the rest of society suffers from untreated excreta disposal (4).

The aforementioned water pollution is mainly provoked by excreta disposal, discharges of oils and fats, microorganisms (bacteria, viruses, and fungi), toxic and radioactive elements, and another common pollutant classified as emerging pollutants, which include dyes, pharmaceuticals, hormones, pesticides, heavy metals, polycyclic aromatic hydrocarbons, and industrial additives, among other sources (5). The treatment or discharge of these contaminants is often not properly regulated; therefore, they are considered a threat to life and the quality of the water (6, 7).

In view of this alarming panorama, drinking water scarcity has become an immense problem, making its purification one of the greatest environmental challenges of recent decades. Currently, some of the wastewater remediation technologies implemented are: activated sludge, chemical precipitation, ozonation, ion exchange, anaerobic digestion, filtration, and adsorption, etc (8, 9). The selection of the appropriate wastewater remediation technology for this purpose will depend on the characteristics of the wastewater to be treated because each method has its own properties such as viability, efficiency, environmental impact, sludge production, operation difficulty, pretreatment require-

ments, and the formation of toxic by-products (9).

In this respect, adsorption is a surface exothermic process where the molecules of a compound in a gaseous or liquid state are accumulated on an adsorbent surface. This process can occur in two ways: physical adsorption, also called physisorption, and chemical adsorption, also known as chemisorption (10). Therefore, one of the most avant-garde technologies at present is the implementation of wastewater treatment with materials that have high adsorption capacity, high surface area and large porosity (11, 12, 13).

Wastewater treatment via adsorption using activated carbon (especially for metals, pharmaceutical compounds, and dyes) is considered a very efficient, and high regeneration capacity technique. However, production of activated carbon is energy-intensive. The adsorption capacity of activated carbons strongly depends on several factors such as pH, concentration of the contaminant to be removed, particle size of activated carbon, temperature of activation, contact time, agitation speed with the contaminant, and the nature and type of precursor (6). Similarly, the particular textural characteristics in terms of surface area and pore distribution, and functional groups present on the surface of the activated carbon could determine the adsorption efficiency, depending on the polarity of the pollutants to be absorbed.

Currently, several solid wastes have been deployed as a sustainable precursors to produce activated carbons. These solid residues include animal waste, lignocellulosic biomass, and, in certain cases, sewage sludge. However, the resulting carbonaceous materials are frequently evaluated under ideal conditions, considering one pollutant and letting aside the main problem to be solved, which is removing multiple pollutants. This makes even more sense when the water's composition is analysed because typically it contains a variety of pollutants from industrial, untreated agricultural, and municipal sources (14).

Hence, this thesis project focuses on the production of activated carbon to be applied as adsorbent using macadamia nutshells as an abundant lignocellulosic precursor. The produced adsorbent was tested in water treatment of emerging pollutants using two pollutant models namely antibiotics (amoxicillin) and dyes (methylene blue) as a binary solution in a single adsorption. Critical analysis to understand the structural-performance relationship of the produced activated carbon were conducted. The effects of pH, temperature, pollutant concentration, contact time, adsorption process's kinetics, isotherm models fitting, and thermodynamics were examined. The reusability of the produced activated carbon was tested using four different methods to regenerate the saturated activated carbon.

1.1 Objectives

1.1.1 General

To develop, and characterize activated carbon from macadamia nutshell for removal of amoxicillin and methylene blue from aqueous solution.

1.1.2 Specific

- To produce activated carbons from macadamia nutshell through chemical activation technique using K_2CO_3 as activating agent.
- To characterize the best adsorbent obtained from experimental design and establish the adsorbent structure-performance relationship for removal of amoxicillin and methylene blue.
- To analyze the effect of the activation factors and optimize the influencing parameters using Box Behnken design.
- To elucidate the adsorption behavior and mechanism using thermodynamic, kinetics, and isotherm models.
- To evaluate the reusability of the activated carbon using four different regeneration techniques.

1.2 Thesis structure

This thesis is made up of six chapters, which contain all the essential information and methods followed to ensure the fulfilment of the objectives mentioned above.
Chapter 2 provides a general review of previous studies and additional information that addresses multipollutant adsorption, the usage of macadamia nutshell as a precursor, and the relevance of the threat to the selected pollutant. Chapter 3 presents a literature review of different concepts and technical information about activated carbon, adsorption processes using this material, the effect of each factor (such as pH, time, and temperature, among others) on the response variable, and its regeneration. Chapter 4 focuses on describing all the methods and techniques used to produce the macadamia nutshell activated carbon and gives details of the adsorption mechanism and the regeneration of the activated carbon. Chapter 5 presents the obtained results, emphasizing the binary solution removal effectiveness according to the different conditions under which activated carbon was produced and the conditions to which adsorption was subjected. Finally, Chapter 6 includes highlights from the thesis work and conclusions.

Chapter 2

Background

Activated carbon is characterised by its porosity, high surface area, and chemical structure, which allows it to present different behaviours depending on the environment in which it is employed (15). These characteristics could be changed according to the precursor, activating agent, and the method employed to produce them. In this sense, activated carbon is produced using various thermochemical processes such as pyrolysis, hydrothermal processes, and gasification in the absence of oxygen (6).

This material is used for more than just wastewater remediation; its properties make it suitable for use in energy storage devices, hydrogen storage devices, soil improvements, pharmaceuticals, food, and odour purifiers, among other things (16). In the last decade, the global production of activated carbon has increased by 5.5% (17). Additionally, it was estimated that its market was valued at $3.43 billion USD in 2021, which shows how important and useful this material is (18). Generally, for commercial purposes, coal, wood, peat, lignite, coconut shell, lignin, petroleum coke, and synthetic high polymers are mainly used as activated carbon precursors, since all of them are rich in carbon (19).

At present, the production and use of activated carbon as an adsorbent have increased significantly (16). Investigations about activated carbon have introduced new materials as precursors and a diversity of options for how these materials can be doped, with the aim of improving their adsorption capacity and ability to work in different media.

Hence, lignocellulosic biomass is also distinguished by its abundance and viability for implementation from an economic viewpoint and in terms of food safety. In this sense, the activated carbon produced from this type of precursor is characterised by high chemical and physical stability (20). Through the use of lignocellulosic materials, it is possible to reduce organic waste and obtain another reusable material, in this case, activated carbon. For this reason, in this work, the production of activated carbon from the macadamia nutshell is proposed, which is considered a residual resource. As an activated carbon precursor, this biomass has not been extensively studied, especially as an amoxicillin adsorbent.

Amoxicillin ($C_{16}H_{19}N_3O_5S$) is an anionic pharmaceutical compound derived from the β-lactam antibiotics of the penicillin class. This antibiotic is widely used in human and veterinary medicine to treat bacterial infections (21). Amoxicillin and amoxi-

cillin/clavulanic acid have been shown to be commonly used drugs around the world, according to the Word Health Organization (WHO) (22), which is why these antibiotics can be identified as a component of the industrial route as well as a compound in urine and feces (23). A study revealed that about 86±8% of consumed amoxicillin by humans is excreted in the urine (24). A significant amount of amoxicillin could be able to produce important health effects such as stomach-ache, skin irritation, diarrhea, antibiotic resistant, nausea, among other symptoms (25).

Also, methylene blue ($C_{16}H_{18}ClN_3S$) is a cationic dye commonly used in the textile industry and employed for medical and veterinary purposes (26, 27). Huge concentration of this compound might affect the enhancement of heart rate, skin irritation, vomiting, headaches, and contamination of the water (28). As previously stated, an anionic (amoxicillin) and a cationic (methylene blue) contaminant were used in this thesis project to investigate competitive adsorption phenomena when the activated carbon comes into contact with pollutants with different polarities. Some previous works focused on the study of the removal of multi-polluted water using activated carbon made from a renewable resource, such as lignocellulosic biomass.

Hence, working with a mixture of contaminants as multipollutant adsorbate represents the real scenario encountered in treatment plants. Also, it poses an important challenge to the researchers to describe the adsorption processes and contemplate the variables that affect adsorption behaviour and kinetics. The study of the behaviour of a mixture of two pollutants (also known as binary pollutants) and activated carbon could be the start of this material's transition to improve its capacities for the entire wastewater treatment process.

In this context, Yiying et al. (29) used avocado seeds to produce activated carbon for the removal of p-cresol and ammonium as a binary solute. The activated carbon was produced via chemical activation with 70% methanesulfonic acid as the activating agent in a 0.8 acid-biomass ratio for 17 h. The resulting material was dried at 95 °C and carbonised at 700 °C for 1.5 h. Their results showed that a maximum adsorption capacities of 87.79 mg/g and 3.393 mg/g for p-cresol and ammonium, respectively could be achieved using their activated carbon.

Chan et al. (30), for their part, conducted chemically activated carbon production using an acid activating agent (H_3PO_4) and waste bamboo scaffolding as precursors to carry out chemical activation, in a ratio of 2.41, respectively. The impregnated material was heated in two steps: the first one for 2 hours at 150 °C and then for 4 hours at 600 °C. As a final step, they wash this new adsorbent material and taste it with Basic Yellow 11 and Maxilon Red 200%, the first of them presents better adsorption affinity with this activated carbon.

Benhabiles and Rida (31), produced activated carbon from sawdust with NaOH to

conduct the chemical activation. Their main objectives were to know how the influence of time, temperature, and ratio during the activation process influence on the final structure of activated carbon and its behaviour in adsorption with a binary mixture composed of erythrosine and methylene blue. Their best material was made with a 1:1 impregnation ratio at 85 °C in 2 h. As a result, they reported adsorption values of 72 mg/g for methylene blue and 65 mg/g for erythrosine in a binary system.

Only a few studies have used macadamia nutshell as a precursor to produce activated carbon, and it was never used to adsorb more than one pollutant. For instance, Martins et al. (32) prepared and characterized activated carbon from macadamia nutshells with NaOH as an activating agent for tetracycline adsorption. They reached a maximum adsorption capacity of 455.33 mg/g.

Wongcharee et al. (33), on the other hand, used a doping of activated carbon and zeolite produced through physical activation (using CO_2 as an activated agent) from macadamia nutshell to adsorb methylene blue, with the best removal relationship obtained in this study being 97 mg/g. According to other related work developed by the same research group (34), they prepared mesoporous activated carbons by carbon dioxide activation to adsorb methylene blue, yielding a material with a removal capacity of 134.69 mg/g.

Dao et al. (35), investigated the use of macadamia nutshell as an absorbent material for wastewater treatment, employing H_2SO_4 and K_2CO_3 as activating agents to remove methylene blue from water.

Hence, this thesis work intends to show and at the same time bring valuable information together about current challenges in the removal of binary pollutants using activated carbon prepared from macadamia nutshell, focusing on absorbent characteristics, modifications, and some drawbacks inherent. Additionally, to look at the entire problem, this thesis also considers the regeneration of the activated carbons previously saturated with a binary solution through four different ways that result in different efficiencies and textural and chemical modifications, among other phenomena to analyse.

Chapter 3

State of the art

3.1 Lignocellulosic biomass

Lignocellulosic biomass residues are organic materials that are part of or comes from flora, which do not represent a threat to the food sector, and it is abundant (36). The purpose of using lignocellulosic materials is to provide a correct CO_2 balance. In other words, CO_2 emissions during production and use must be equal to CO_2 consumption during plant life (37).

Today, the use of these materials is important in the industry because it is possible to reduce organic wastes and greenhouse gases emissions while also obtaining products such as chemicals, biofuels, and other value-added products (38). This type of biomass includes grasses, soft and hard woods, and, as well, any type of agricultural waste and certain industrial wastes.

Lignocellulosic biomass is mainly composed of lignin (10–25%), cellulose (35–50%), and hemicellulose (20–35%). Also, there are other compounds in lesser proportion such as extractives, ash, proteins, etc. (39). The proportions of these compounds vary depending on the lignocellulosic resource and could influence the structure and properties of activated carbon.

Lignin is a highly cross-linked aromatic polymer mainly composed of phenylpropane units. The principal building blocks of lignin are *p*-coumaryl, coniferyl, and sinapyl alcohols (Figure 3.1). All these units are linked by ether bonds, carbon-carbon bonds, and ester bonds, the first of which constitute 60%-70% of the total linkages, being the most common of this specie β-O-4 linkage (40). Lignin's primary function is to provide structure, strength, protection from environmental factors (such as sunlight, blizzards, and snowfall), and resistance to biological attacks, among other things (41, 42). As an isolated component, lignin is used to produce vanillin, dispersant, emulsifier, fertilizers, and herbicides, etc. Research is primarily focused on developing energy, macromolecules, and aromatic compounds (43).

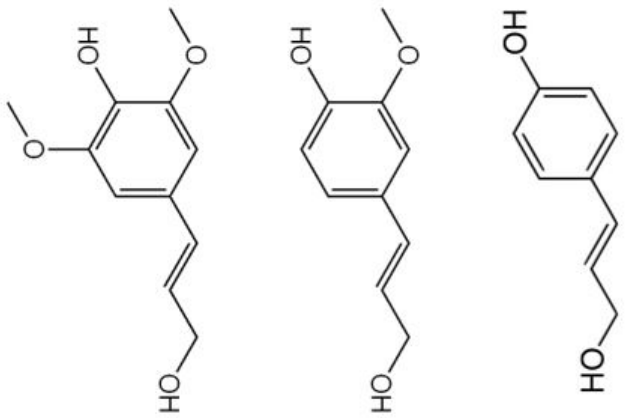

Figure 3.1: Precursors of lignin. From left to right: sinapyl alcohol, coniferyl alcohol y *p*-coumaryl alcohol.

Cellulose is the most abundant polymer in nature, mainly composed of D-glucopyranose units linked through β-1,4-glycosidic bonds (44). Its general formula is represented by $(C_6H_{10}O_5)_n$ (Figure 3.2), and its polymerization degree is between 9000 and 10,000 Da. This polysaccharide could form hydrogen bonds because of the existence of hydroxyl bonds in the glucose molecules (C6, C2, and C3), which promote the construction of the structure from chains onto a fiber (45, 46). These cellulose microfibrils are primarily wrapped by other biopolymers such as lignin and hemicellulose, resulting in the complex structure of lignocellulosic biomass, which presents a challenge when attempting to isolate any of these components (47, 48).

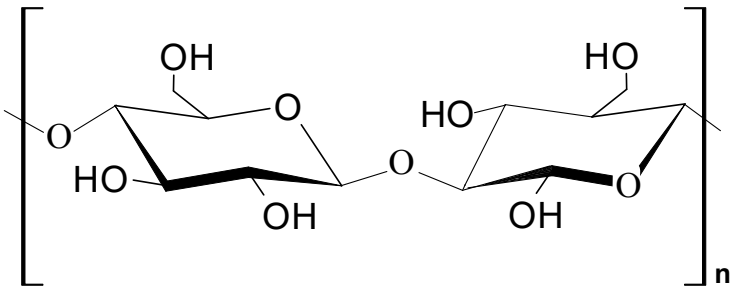

Figure 3.2: Chemical structure of cellulose.

Hemicellulose, is a short chain polymer mainly composed of heterogeneous monomers with amorphous structure (hexoses and pentoses), among them, it is possible to find xilose, manose, arabinose, galactose and glucose (Figure 3.3); additionally, it is possible to find acetyl groups and glucuronic acid (49). Hemicelluloses xyloglucan chains are the

most abudant in biomass, they are represented in almost 20-30% of the forest biomass and approximately 50% on the grass biomass (41).

This component of the biomass connects with the cellulose structure through Van der Waals forces and hydrogen bonds (50). Hemicellulose is usually required for the production of cosmetics, biofuels, xilitol, and sugar conversion processes (i.e., fermentation processes), to name a few (51).

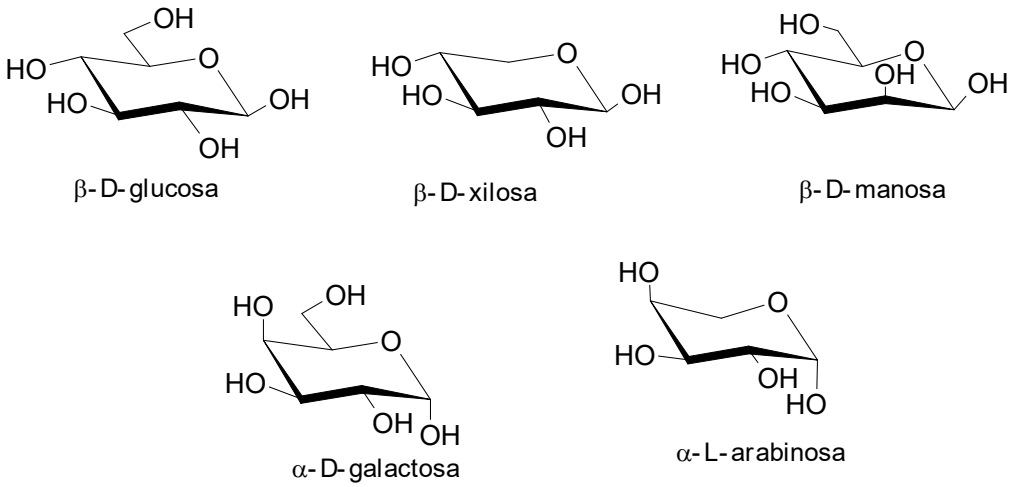

Figure 3.3: General structures of hemicellulose.

3.1.1 Macadamia nutshell generalities

Macadamia integrifolia is a native tree that originated in New South Wales and Queensland, Australia. The macadamia nut tree was given its scientific name in recognition of an Australian scientist, John McAdam (52, 53). The macadamia nut tree can grow up to 15 metres tall and 6 to 12 metres in diameter. Its fruit ripens 6 to 7 months after flowering; the complete fruit (seed, husk, and shell) measure between 2.6 and 5 cm in diameter (54, 55). In industry, 60% of this product is mainly used in cosmetics or medications, and the remaining 40% is destined for the food industry (55).

The worldwide production of macadamia nuts registered in 2019 was about 60,057 metric tonnes (on a kernel basis), with South Africa (29%), Australia (22%), and Kenya (12%) being the principal producers (56). More recently, data from 2021 show that the production on the same scale was around 369,491 tons (57). In Mexico, however, the production of this crop reached approximately 32,205.77 tons, with Puebla, Veracruz, and Chiapas being the main Mexican states producers (58).

Considering that the shell constitutes a third part of the complete fruit, the statistics mentioned above could highlight the large quantity of macadamia nut residue obtained (53). The macadamia nutshell (Figure 3.4) is made up of two layers: the internal one is softer and more flexible, which protects the fruit, while the external one is extremely hard and hydrophobic, with a thickness that oscillates between 1.5 mm and 5 mm (59). The macadamia nutshell is employed as feed livestock, the production of various sorts of plastics, as well as for covering nurseries, fuel, and composting (60).

Figure 3.4: Macadamia nutshell biomass.

3.2 Lignocellulosic biomass to produce activated carbon

Biomass transformation is an important step that must be taken in order to obtain materials with specific properties or to benefit from some biomass components over others. Biomass conversion can be classified into biological (digestion, fermentation) and thermochemical process (hydrothermal processing, pyrolysis and gasification), the main goal of this treatment is to transform the original biomass into chemicals and solid, liquid and gas fuels (40).

In this sense, pyrolysis promotes the thermal degradation of biomass at high temperatures (typically between 300 and 1200 °C), and in the absence of oxidising agents, the decomposition of the biomass occurs due to the material's unstable chemical bonds (61). Pyrolysis could provide three products in different aggregation stages: solids (such as charcoal, biochar, and ashes), liquids (typically tars, heavier hydrocarbons, and water), and gases (CO_2, H_2O, CO, C_2H_2, C_2H_4, C_2H_6, and C_6H_6) (62, 63).

Additionally, pyrolysis may occur as slow pyrolysis (carbonization and torrefaction) or fast pyrolysis (flash and ultrarapid). The selection of the method to carry out depends totally on the results to be achieved (64). Thus, the principal product obtained from slow pyrolysis is charcoal, or char. Flash pyrolysis is used to produce bio-oil, chemicals, and gases. Ultrarapid is mainly used to obtain gases and chemicals (65). The main characteristics of each type of pyrolysis are described in the Table 3.1 showed below.

Table 3.1: Pyrolysis characteristics classification.

Pyrolysis technique	Time	Temperature range (°C)	Heating rate (°C min^{-1})	Ref.
Torrefaction	30-120 min	200 - 300	<50	(66)
Carbonization	Hours/days	>400	<80	(67)
Ultrarapid	<0.5 s	1000	>60,000	(68, 69)
Flash	<1 s	800 – 1000	>30,000	(68, 70)

Currently, it is well known that biomass composition influences the activated carbon characteristics and yield in a thermochemical process. In other words, during pyrolysis, each component of lignocellulosic biomass reacts differently (71). This is due to the thermal stability of the main components of lignocellulosic biomass. For example, lignin is a biopolymer whose decomposition occurs between 200 °C and ∼ 1000 °C (72); similarly, hemicellulose decomposes in the range of 200-350 °C (73), and cellulose degrades between 250 and 370 °C (74).

Besides, during the pyrolysis, linkages present in lignin structures such as β-O-4 could be easily broken at relatively low temperatures (200-250 °C, in this case), promoting the formation of the carbon-like characteristic solid structure. The decomposition of cellulose depends on the temperature: at low temperatures, it turns into anhydrocellulose which promotes a high carbon content, while at high temperatures, it turns into volatile products (40, 75). Hemicellulose, is mainly converted into volatile products (17).

The production of activated carbon also includes the activation process, apart from pyrolysis (carbonization). In this sense, the pyrolysis promotes the construction of the elemental carbonaceous structure and by applying the activation stage, the pore features are improved (76). Activation could happen mainly by physical or chemical activation; however, physicochemical and microwave-assisted activation are also applied but to a lesser extent.

Carbonization and activation by separate stages are included in physical activation, which means that the biomass must be carbonised (400-700 °C) in an inert atmosphere before pyrolysis (800-1100 °C) with an oxidising agent such as steam, air, or CO_2. On

the other hand, using chemical activation makes it possible to carry out carbonization and activation at the same time using chemicals as activating agents (NaOH, KOH, $ZnCl_2$, and H_3PO_4) and applying temperatures between 400 to 1000 °C (77, 78).

The conditions applied to produce activated carbon determine its characteristics (such as pore size and volume, surface area, chemical inertness, and stability), regardless of the properties of the biomass. In this sense, these activated carbon properties depend directly on the biomass particle size, temperature, activated agent proportion, and heating rate used during the thermochemical process (pyrolysis, in this case) (79). It is critical to consider these factors in order to obtain materials that are more suitable for final application, such as adsorption.

For instance, the pore size distribution and volume mostly depend on the activating agent, which describes the affinity between the pollutants and emphasises the mechanism of competition in a multi-pollutant system. Similarly, the biomass particle size determined the surface area of activated carbon; hence, the adsorption efficiency is higher when the particle size is smaller (71).

3.3 Adsorption

Three main elements describe the adsorption processes: adsorbent, adsorbate, and medium. Adsorbents are materials with a high volume and surface area that can remove interest compounds from a given medium through processes that occur only on their surface. In simple terms, adsorption is defined as the mass transfer of an adsorbate from a specific medium onto the surface of an adsorbent (80). The most important applications of this technique are to remove pollutants from the air and for wastewater treatment.

The nature of the interactions that occurs between adsorbate-adsorbent define their mechanism, which can be categorized as chemical adsorption (or chemisorption) and physical adsorption (or physisorption) (81). Chemisorption is characterised by the formation of strong bonds as a consequence of electron exchange or transfer between the adsorbate and the surface site. Usually, this involves ionic or covalent bonds. In this type of adsorption, the adsorbate forms a monolayer on the adsorbent, requires a high energy (40 to 800 kJ/mol), and is stable at high temperatures. All of these characteristics imposes difficulty in the desorption process.

On the other hand, attraction forces between the adsorbate and the adsorbent defined as the physisorption process is due to electrostatic forces, hydrogen bonding, Van der Waals, or dipole–dipole forces. Usually, it requires a low adsorption energy (5 to 40 kJ/mol) and reaches stability at low temperatures, which permits an easily reversible desorption (80, 82).

3.3.1 Adsorption kinetics

Understanding the adsorption kinetics (Figure 3.5) could help to obtain information about the adsorption rate, data from the conditions where equilibrium is reached, the adsorbent behaviour, and especially to describe mass transfer mechanisms. The adsorption kinetics includes principally four steps: bulk phase, external diffusion, internal diffusion, and adsorption of adsorbate on active sites (83, 84).

First, in the bulk phase, the adsorbate atoms approach the surface of the adsorbent. Then, in the external diffusion, the transference between the liquid phase and the surface of the adsorbent initiates. After that, in the internal diffusion, the textural characteristics of the adsorbent play a very important role. In this step, the adsorbate diffuses into the pores or surface of the adsorbent. The last stage considers the adsorption mechanism; depending on how the adsorbate and the adsorbent interact, it could be chemisorption or physisorption (85, 86).

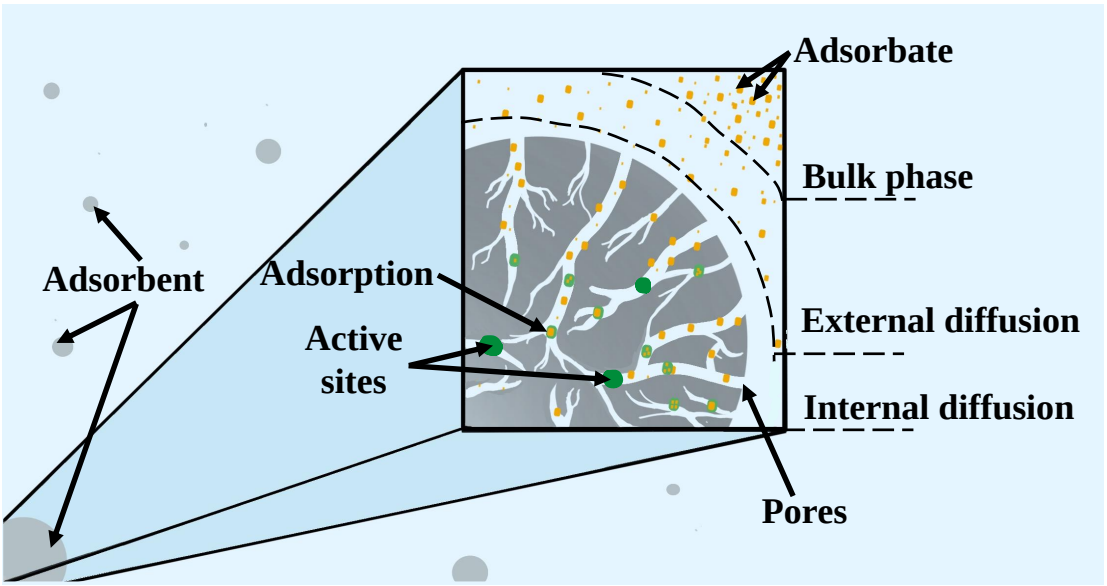

Figure 3.5: Adsorption kinetics steps.

Typically, pseudo-first-order (PFO), pseudo-second-order (PSO), Elovich, and Weber-Morris intraparticle diffusion models are used to help to describe and identify the adsorption mechanism of a particular experiment. All of them have different physical meanings, and their interpretation depends on how well they fit the experimental data provided. To test the already mentioned fits, it is important to prove the correlation through multiple error calculations such as the coefficient of determination (R^2), average relative error (ARE), and root-mean-square error (RMSE), among others.

3.3.1.1 Pseudo-first-order (PFO)

In 1898, Lagergren proposed this model, especially for solid-liquid systems. His work considers that the adsorption rate is proportional to the difference between the free active sites and the saturation concentration (87). The pseudo-first-order kinetics model assumes that the adsorption is governed by a non-reversible reaction where only adsorbent features are responsible for the process, that is, discarding the adsorbate-ion interaction influence (88). The Lagergren pseudo-first-order model could also be suitable for overdose solution experiments (89) and provide an adequate model for the initial adsorption phase (90). Usually, this model is related to physisorption adsorption mechanisms.

Starting from a differential equation, it is possible to find all the variables that control the adsorption, which include the amounts of the adsorbate adsorbed, taking into account the time and also an equilibrium rate constant. The equation of this model could be consulted in next chapter (Equation 4.5). The already mentioned variables are mostly founded on the linearization of the equation; however, many authors have observed that errors could be propagated through this methodology (91).

3.3.1.2 Pseudo-second-order (PSO)

The model was proposed in 1995 by Ho and is suitable for low-concentrated solutions (92). It assumes that the mechanism involved is clearly chemisorption and that its adsorption capacity primarily depends on the chemical characteristics of the adsorbent (i.e., functional groups) (80). According to the literature, this fitting could be capable of being adapted during all steps of the adsorption processes, and through the calculations, it is possible to obtain all the parameters of the equation, in contrast to the pseudo-first-order model (86).

The pseudo-second-order kinetics model is developed to establish a proportionality between the adsorption rate and the adsorption capacity (91). In this sense, the already mentioned model plays an important role in adsorbing dyes, metal ions, oils, and organic substances, all of which are diluted in water (83).

3.3.1.3 Elovich

This model was developed by Zeldowitsch in 1934; his experiment consisted of describing the behaviour between carbon monoxide and manganese dioxide (93). According to the nature of the Elovich experiment, his model could lend validation to a pseudo-second-order model while assuming chemisorption as the principal adsorption mechanism. Also, the model considers an heterogeneous adsorbent surface in terms of energy and states that the adsorbate concentration decreases exponentially as a function of the increment in the amount adsorbed (94). Usually, the Elovich model is widely applied to

the adsorption of gases, metal ions, organic pollutants, and to the removal of pollutants in aqueous solutions (85).

3.3.1.4 Weber-Morris intraparticle diffusion

Diffusion models are another way to describe adsorption kinetic processes, which, in contrast with the traditional models (PFO, PSO, and Elovich), are based on mass conservation principles and kinetics laws. As a result, using diffusion models eliminates the experiment's specific conditions, such as initial adsorption rate, desorption rate, and equilibrium adsorption rate. The previously mentioned assumption establishes direct knowledge of the kinetics of the adsorption phenomenon itself as well as the mass transfer process between adsorbate and adsorbent (95, 96).

At the same time, diffusion models could be divided into internal and external diffusion; the Weber-Morris model is part of the first group. Internal diffusion models indicate that this step is the slowest part of the adsorption (85). In this sense, the Weber-Morris model is described through a nonlinear equation (Equation 4.8) that clearly represents the multiple factors that may influence the adsorption rate (86).

3.3.2 Adsorption isotherms models

Adsorption isotherms are mathematical models that describe how pollutants interact with the adsorbent material. These models provide information about the maximum adsorption rate, describe the adsorption pathways, and, more importantly, provide more understandable knowledge about how to optimise adsorption process (85, 97). The adsorption isotherms come essentially from experimental data performed at constant temperature and pH. Its mathematical formulation starts by assuming that adsorption and desorption rates reach equilibrium and also takes into account the thermodynamic parameters (98).

Adsorption isotherms may be classified as functions of the parameters to be found using their own equations. There are two to five parameters, and multilayer physisorption isotherms. In practice, it is common to use more than one isotherm model for a single experiment with the aim of abstracting all the possible physical correlation meanings (97). The Langmuir, Freundlich, and Temkin models are commonly used to describe adsorption processes. However, the use of these models can vary according to the experimental characteristics.

3.3.2.1 Langmuir isotherm model

The Langmuir (1916) isotherm is one of the earliest developed isotherm models and is currently widely used to describe the adsorption of pollutants in aqueous solutions. Originally, this model was developed to describe a gas-solid system, assuming ideal

behaviour of both the adsorbent and the adsorbate (99). Its mathematical formulation considers monolayer coverage on a homogeneous surface; that is to say, the adsorption only happens onto definite and located active sites: one molecule is adsorbed to only one active site (97). Furthermore, the model ignores lateral interactions from adsorbed molecules and also assumes that the adsorption energy is constant (100).

The Langmuir model has two constants: one of them represents the maximum adsorption capacity, and the other one describes the surface properties of the adsorbent (affinity constant). To get all of these parameters, it is often necessary to use the linearization of the original equation. There are at least four ways to linearize the Langmuir equation, but all cases may lead to errors (101). Currently, a significant quantity of isotherm models are inspired by and founded on the Langmuir isotherm, among which we can find Jovanovich, Koble–Corrigan, Marczewski–Jaroniec, Baudu, Brouers–Sotolongo, and Khan, just to name a few. All of the models already mentioned are characterised by the ability to modify and improve the description of the adsorption processes (102).

3.3.2.2 Freundlich isotherm model

Contrary to the main assumptions that govern the adsorption process described by Langmuir, the Freundlich isotherm model is designed for multilayer systems adsorbed on heterogeneous active sites (103). The model was developed by Freundlich in 1906, to describe animal charcoal adsorption. In this experiment, it was observed that the adsorption was not constant when the ratio of adsorbent to adsorbate was modified (104). Due to its nature, the Freundlich model was the earliest to describe a non-ideal and reversible case of adsorption. Even more, the model declares that the active sites of the adsorbent have different energies (heat), but the entropy remains constant for all of them (91).

Through their mathematical parameters, the equation provides knowledge about the heterogeneity of the active sites, the energy distribution of the adsorbent, and the surface coverage (98). The Freundlich model is widely used to describe the adsorption of organic compounds, dyes, and heavy metals on activated carbon (105). Otherwise, some of the limitations of the Freundlich model consist in its impossibility to give the correct interpretation of the adsorption mechanism at a molecular level, in addition to the propagation of errors caused by the logarithmic function intrinsic to the model equation (91).

3.3.2.3 Khan isotherm model

The Khan isotherm was a mathematical model developed in 1996 that included singularities from the Langmuir and Freundlich isotherms (106). In their work, Khan et al. used experimental adsorption data from the literature to propose a reliable method

capable of describing the adsorption of multi-component and organic solutes using activated carbon as an adsorbent. With this context, this model is considered appropriate to describe adsorption systems in which pure solutions (bi-adsorbate) are involved (102).

Also, Khan is categorized as a 3-parameter isotherm model, which allows showing the influence of the experimental conditions while reducing the propagation of errors in aqueous adsorption systems (107). The Khan parameters include the maximum adsorption capacity of the specific experiment, the Khan constant, and the exponent of Khan, which could determine the relationship degree to the Langmuir or Freundlich isotherms (108).

3.4 Factors that influence adsorption processes

As mentioned in previous sections, several factors can influence the adsorption behavior of activated carbon, including pyrolysis and adsorption conditions, as well as the adsorbate with which it comes into contact. More specifically, these factors may influence the textural (surface area and pore structure), chemical (functional group and elemental composition), and behavioral properties of the activated carbon.

Characterization methods exist that can analyze and inform about the properties of a specific activated carbon. Through these methods, it is possible to understand and enhance the adsorbent attributes. In this sense, scanning electron microscopy (SEM) provides micrographs of the textural morphology of the adsorbent; on the other hand, fourier transmission infrared spectroscopy (FTIR) gives us information about the functional groups of the analyzed materials; and physisorption equipment provides surface area and pore size distribution data using the nitrogen cryogenic properties (109). In the following sections, there is an overview of the variety of features that may affect the efficiency of adsorption processes.

3.4.1 Activated carbon properties

Textural and chemical surface properties of activated carbon are defined as a result of the intrinsic properties of the biomass and the conditions under which it was produced. From this perspective, the chemical properties of the activated carbon are linked to its surface functional groups, which impact the porous properties of the adsorbent, the surface charges, and the adsorption characteristics (110). These functional groups result from the union between the heteroatoms (hydrogen, oxygen, sulfur, phosphorus, nitrogen, etc.) and the activated carbon structure, which results in their main functionalities: carboxyl, carbonyl, phenols, lactones, and quinones, among others (111). Thus, its classification depends on the nature of the heteroatoms present in the adsorbent, which are divided into oxygen-containing, nitrogen-containing, and sulfur-containing functional groups (112).

Despite the fact that the functionalities may improve the adsorption in many cases, it can happen the opposite in others. This means that the adsorbate may not always be compatible with the functional groups of activated carbon. In this sense, pH is an external factor associated with the experimental conditions that has the potential to change the behavior of the functional groups (113). Currently, there are some modification methods that help to improve the adsorption properties throughout the functional groups of the activated carbon, which are: oxidation, nitrogenation, sulfuration, ammonification, among others (114).

On the other hand, textural properties mainly result from the activation stage of the activated carbon, which may happen in a chemical or physical way. In this sense, these textural characteristics are associated with the specific surface area, pore volume, and size distribution. Usually, high values in a specific area enhance the adsorption capacity level because, in this way, the probability of accessing more active sites is increased (115).

These active sites are related to the pore structure of the adsorbent (Figure 3.6), which is classified as micropores (<2 nm), mesopores (2–50 nm), and macropores (>50 nm). The micropores make up the majority (< 90%) of these adsorption sites (116). Furthermore, the literature indicates that carrying out chemical activation is most likely to obtain microporosity as the principal textural characteristic (71). Mesoporosity, for its part, works as a transition stage that permits the access (slowly) of the adsorbate to micropores, and macropores, aside from being the ones that contribute the most to the pore volume, are the ones that let the adsorbate enter quickly to the active sites (117).

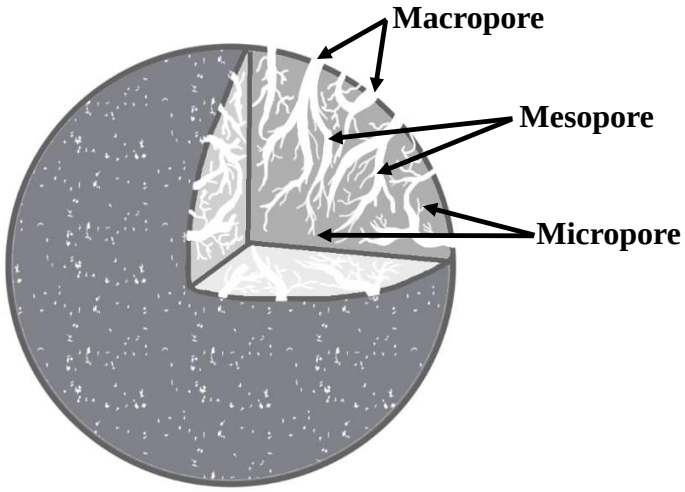

Figure 3.6: Pore classification according to the size.

3.4.2 Adsorption experimental conditions

It is critical to examine the experimental conditions in order to improve the adsorbent-adsorbate interactions, which reflect the degree of removal. These conditions include pH solution, temperature, pollutant concentration, and contact time. Thus, pH of solutions play an important role in controlling the electrostatic forces between adsorbent and adsorbate by regulating the charge on the surface of the adsorbent. The pH could interact with the heteroatoms and change the functionalities presented on the adsorbent (82). In addition, by using the pH of the point of zero charge (pH_{pzc}), it is possible to determine the charges (positive or negative) on the surface as a function of pH. The value of the pH_{pzc} establishes the pH, where the positive and negative charges are balanced, which means there is a neutral charge (118).

Otherwise, controlling the temperature along the experiment affects the mobility of the adsorbate molecules in the solution to be adsorbed; as a consequence, a high temperature level promotes the diffusion of the adsorbate throughout all the adsorption steps (119). However, increasing the temperature of the adsorption process has an upper limit; passing over this peak causes a decrease in the effectiveness of the adsorption (120). In other words, temperature regulates the adsorption rate and removal percentage.

Contact time is also an important parameter to be regulated in adsorption experiments. Studying this factor helps determine the minimum time required for adsorbate and adsorbent to reach equilibrium (120). The contact time could vary depending on the adsorbent characteristics (chemical and textural) (121). On the other hand, the initial concentration of the adsorbate is extremely related to the contact time; that is, as the initial adsorbate concentration increases, so does the contact time with the adsorbent (31). At the same time, control the initial concentration of the pollutant and determine the removal capacity of the adsorbent.

3.5 Regeneration

After using activated carbon in various adsorption methods, the spent carbon could be discarded or recovered through regeneration and reactivation (122). Particularly, to regenerate saturated activated carbon, there are different methods to achieve that. The most common are thermal regeneration, wet air oxidation, solvent regeneration, and chemical regeneration; however, there are also microwave-assisted, electrochemical, and biological methods, which are less commonly used (123).

The appropriate regeneration technique is determined by the adsorption mechanism observed during the experimental behaviour of a specific activated carbon species, namely chemisorption or physisorption. It is remarkable that adsorption behaviour is affected

by adsorbate qualities and adsorbate affinity (6). Table 3.2 summarizes some of the previously mentioned regeneration methods' characteristics.

Table 3.2: Common activated carbon regeneration methods.

Regeneration technique	Reagents employed	Time of reaction	Temperature range	Reference
Thermal regeneration	Inert atmosphere (N_2, CO_2, etc.)	20-60 min	Three stages: 1) 200 °C, 2) 400-600 °C and 3) 800-1000 °C	(124)
Wet air oxidation	O_2 or air stream	2-4 h.	125-320 °C	(125, 126)
Solvent regeneration	Methanol or acetone	>1h	30-50 °C	(6)
Chemical regeneration	HCl, H_2SO_4, HNO_3, NaOH, H_2O_2	>1h	Room temperature	(127, 128)

In this thesis project, chemical and solvent regeneration was used because these methods have not been widely used and according to the literature they cause less damage to the porous structure. Chemical regeneration is one of the most used methods for regeneration of spent activated carbon. This method, as its name suggests, involves the employment of chemical reagents that interact with the adsorbate and either change its composition or influence equilibrium adsorption, which in both circumstances allows the promotion of desorption (129, 130).

The level of regeneration attained with this method is highly dependent on the acid-base or redox reactions produced by the adsorbate affinity with the chemicals employed (131). Chemical regeneration has a number of advantages over other approaches, including lower mass losses, and on the other hand, the adsorbate may be recovered using some separation techniques (132). Furthermore, the use of this technique promotes the modification of activated carbon's textural properties, i.e., the increase of surface area and the formation of new pores (122).

On the other hand, solvent regeneration promotes the alteration of the electrostatic structure built between the adsorbent and the adsorbate so that the hydrogen bonds and $\pi - \pi$ bonds may be affected, thereby promoting the desorption (133). This method is frequently used to treat wastewater, particularly wastewater that contains metal ions (134). Some advantages of solvent regeneration fall under the category of easy recovery (both adsorbate and solvent). The process is quicker than others and the textural properties are unchanged; additionally, the temperature employed is generally below 100 °C (135).

Chapter 4

Methodology

The present thesis work focused on the use of macadamia nutshell (MNS) as a lignocellulosic precursor to produce activated carbon (AC). The carbonaceous material was produced through the employment of a 3^k Box-Behnken experimental design with K_2CO_3 as activating agent. From the resulting material, each sample produced was selected as a function of the yield and removal percentage. The removal percentage was tested with a solution composed of two emerging pollutants: amoxicillin (drug) and methylene blue (dye), also known in this work as a binary solution (BS). The effects of temperature, pH, contact time, initial concentration of adsorbate, and activated carbon dosage were evaluated. The textural and chemical analysis of the surface of the selected sample was performed.

Additionally, the experimental data was modelled using kinetics models, eight isotherm models, and thermodynamics for a better understanding of the behavior of the process. Finally, four techniques were employed to regenerate the saturated activated carbon, which are classified as chemical and solvent regeneration. Figure 4.1 shows a graphical abstract, which includes the steps already mentioned. The procedures and approaches used for this thesis project are described in detail in the following sections, along with information on the equipment, supplies, and reagents used.

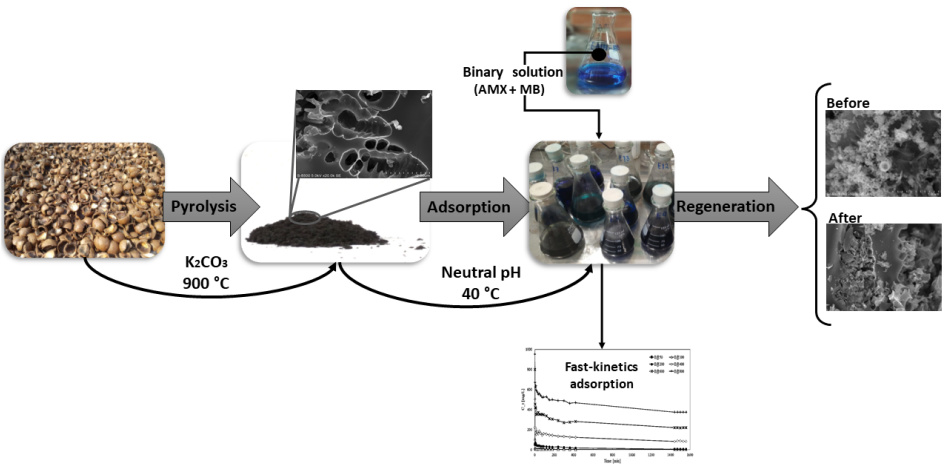

Figure 4.1: Graphical abstract.

4.1 Activated carbon production

To evaluate the effects of activation factors on the textural-morphological characteristics of the activated carbon and their resulting adsorption properties, a Box-Behnken experimental design was used. The factors contemplated to be evaluated were the K_2CO_3:precursor ratio (x1), the activation temperature (x2), and the time of the process (x3). In Table 4.1, the complete experimental design conditions are specified.

Table 4.1: Levels of experimental factors in Box-Behnken design.

Levels	K_2CO_3:Precursor (x1)	Temperature, °C (x2)	Activation time, h (x3)
High (+1)	3:1	900	2
Medium (0)	2:1	800	1.5
Low (-1)	1:1	700	1

The Box-Behnken experimental design prevents material and reagent waste while also allowing for their examination under milder conditions. In this sense, the factorial 3^k design results on fifteen experimental runs, three of them correspond to central points with which the reproducibility and consistency of the data obtained can be correlated.

Chemical activation was used to produce activated carbon in accordance with the experimental design specifications. To do that, 20 g of crushed macadamia nutshells were impregnated with K_2CO_3 in a weight ratio ranging from 1:1 to 1:3 (K_2CO_3:precursor) and diluted in 200 mL of deionized water at 85 °C for 4 h under vigorous stirring. After that, the impregnated macadamia nutsell were dried in an oven at 105 °C overnight to remove excess moisture.

The activation process was carried out in an electrical tubular furnace (Linderberg Blue M) under an N_2 atmosphere flux of 100 mL/min at the temperature specified by the experimental design (700-900 °C), maintaining a heating rate of 20 °C/min, and a residence time of 1-2 h (Figure 4.2). The resulting carbonaceous material was washed using 1M HCl and then deionized water. The purpose of this step was to remove all the impurities and leave the pores available to carry out the adsorption. The washing process was extended until the sample reached a neutral pH and then dried it in an oven at 105 °C for 24 h. With each sample ready, the yield of the activated carbon was calculated using Equation 4.1.

$$Yield(\%) = \frac{MNSAC(g)}{MNS(g)} \times 100 \tag{4.1}$$

where MNS represents the macadamia nutshell lignocellulosic biomass and MNSAC is the amount of activated carbon obtained from each experiment. It is worth mentioning

that the results obtained from the activated carbon yield were analyzed using the ANOVA analysis model with a confidence level of 0.05. All of this concerns the factors included in the experimental design.

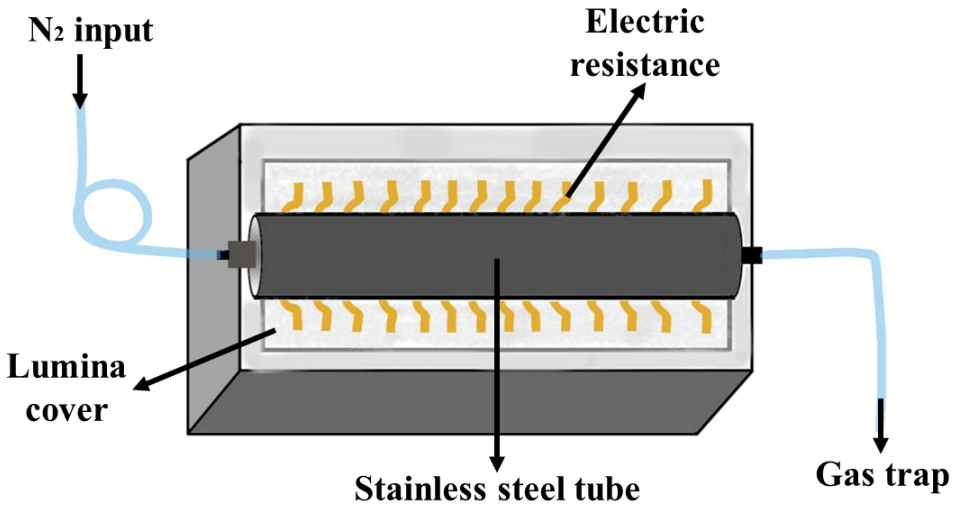

Figure 4.2: Tubular furnace used to activate the impregnated biomass.

4.2 Activated carbon characterization

The characterization of activated carbon was done to understand its intrinsic properties. To achieve this goal, the carbonaceous samples with the best behavior were characterized using a Scanning Electron Microscopy (SEM) S-5500 (Hitachi) model series. With this equipment, it was possible to obtain information about the morphology of the samples, which were analyzed at different magnifications from 15000X to 50000X. In the same way, energy dispersive X-ray spectroscopy (Bruker) (integrated in the SEM) was also used to achieve the elemental analysis.

Additionally, Fourier transform infrared spectroscopy FTIR (Nicolet iS50), was implemented to evaluate the functional groups associated with the adsorbent. The analysis was run in the wavelength range from 4000 cm^{-1} to 400 cm^{-1}. Furthermore, the textural characterisitics were elucidated using the nitrogen physisorption isotherm at 77 K. This procedure required the use of Nova 2200e Quantachrome equipment to determine the specific surface area, which was calculated using Brunner-Emmett-Teller (BET) and Density Functional Theory (QS-DFT) models, by using the NovaWin® software.

4.3 Calibration curves

For elaboration of the BS calibration curve, it was necessary to carry out previous studies of MB and AMX individually throughout the entire absorbance range allowed by the measurement instrument. Based on this information, it was possible to detect that MB had a high absorbance level at ∼664 nm and emitted a small signal in the higher absorbance range of AMX (∼230 nm). Faced with this scenario, in order to obtain the correct quantification of BS, the absorbance at 230 and 664 nm was measured, taking into account adding equal amounts of both AMX and MB. Thus, it was easier to obtain a signal equivalent to the known concentrations of each compound in the BS.

In general, absorbance measurements of AMX and MB (individually) are indispensable for the detection and identification of signals throughout the absorbance range. Likewise, measurements of the BS with AMX and MB at equal concentrations were useful for the quantification of these compounds, taking into account the interferences. The resulting calibration curves are shown in Figure A.1.

4.4 Batch adsorption experiments

To prepare the binary solution (BS) necessary to test the removal capacity of the activated carbon samples, amoxicillin (AMX) and methylene blue (MB) were dissolved in deionized water at the same concentration. In this sense, for a total of 400 mg/L BS, 200 mg/L of MB and 200 mg/L of AMX were added. Then, 0.1 g of each activated carbon sample from the Box-Behnken experimental design was put into a different 125-mL Erlenmeyer flask to conduct batch experiments. Hence, 100 mL of the 400 mg/L BS was added to the all containers. The samples were inserted in a thermostat shaker (Julabo-SW series) and agitated at 150 rpm for 12 hours at room temperature.

Following the completion of the exposition time, a sample of the solution was collected from each experiment to determine the final concentration (Figure 4.3). This residual concentration was determined using a Shimadzu UV-1900 UV-visible spectrophotometer in accordance with a previously created calibration curve for BS, which includes the lecture at 230 and 664 nm (using the respective correction factors). The percentage removal was calculated using Equation 4.2.

$$Removal(\%) = \frac{C_0 - C_f}{C_0} \times 100 \tag{4.2}$$

where C_0 is considered as the sum of the initial concentrations of the BS components (that is $C_0 = C_{0,MB} + C_{0,AMX}$) and C_f ($C_f = C_{f,MB} + C_{f,AMX}$) refers to final concentration of BS in mg/L, respectively. The sample with the best performance was chosen by calculating the removal percentage of each run from the entire experimental design and correlating it with the yield results.

Figure 4.3: Batch adsorption experiments after 12 hours of reaction.

4.5 Influence of pH and pHpzc value

The pH assessment was applied only for the best activated carbon sample. To determine the influence of pH, six reactors were prepared with 0.1 g of the best carbon sample, 100 mL of 400 mg/L of BS, and placed in a 125-mL Erlenmeyer flask. The solution pH of each reactor was adjusted using to pH 2, 4, 6, 8, 10 and 12 using 0.1 M NaOH and 0.1 M HCl.

After that, these six experiments were placed in the thermostat shaker (Julabo-SW series) and agitated at 150 rpm for 24 hours at 30 °C. The initial and final BS concentration and pH were measured by Shimadzu UV-1900 UV-visible spectrophotometer and Sper Scientific Benchtop Meter potentiometer, respectively. The point of zero charge pH_{pzc} was determined using the pH data collected from all the reactors, by graphing the initial pH (pHi) vs. the final pH (pHf). The intersection of these two curves defines pH_{pzc}, which is pHi=pHf.

4.6 BS adsorption equilibrium and kinetics studies

To perform the adsorption kinetics, BS at different concentrations were prepared: 50 mg/L, 100 mg/L, 200 mg/L, 400 mg/L, 600 mg/L, and 800 mg/L. About 200 mL of each BS concentration was placed in a separate 250-mL Erlenmeyer flask, and 0.2 g of the best MNSAC sample was added. The initial concentration was recorded from every single reactor before starting the kinetics studies. To do that, all the flask properly prepared were heated at 30 °C for 24 h under constant agitation at 150 rpm. Through-

out the adsorption period, measurements about the concentration of the solution were taken at different time intervals. All the procedures already described were repeated for temperatures of 40 °C and 50 °C. In this sense, the amount of BS adsorbed at time in mg/g (q_t) was determined from Equation 4.3.

$$q_t = \frac{(C_0 - C_t)V}{W} \tag{4.3}$$

where V (L) is the volume of the BS solution, W (g) is the weight of the MNSAC best activated carbon sample added, and Ct (that is, $C_t = C_{t,MB} + C_{t,AMX}$) is the concentration at time t in mg/L. When the adsorption process (q_e) reached equilibrium, it was also possible to calculate the quantity of BS adsorbed at this point using the concentration at equilibrium ($C_e = C_{e,MB} + C_{e,AMX}$), as shown in Equation 4.4.

$$q_e = \frac{(C_0 - C_e)V}{W} \tag{4.4}$$

Kinetics studies were estimated, taking into account all the concentration data collected for each reactor evaluated at this stage. To accomplish that, all the q_t and q_e data were fitted to the pseudo-first order (PFO), the pseudo-second order (PSO), and Elovich models, which are shown in Equations 4.5 (87), 4.6 (92), and 4.7 (93).

$$PFOq_t = q_e(1 - e^{-k_1 t}) \tag{4.5}$$

$$PSOq_t = \frac{k_2 {q_e}^2 t}{1 + k_2 q_e t} \tag{4.6}$$

$$Elovichq_t = \frac{1}{\beta}\ln(\alpha\beta) + \frac{1}{\beta}\ln(t) \tag{4.7}$$

where k_1 (1/min) and k_2 (g/mg·min) are the rate constants for PFO and PSO, calculated using their respective models. The Elovich kinetics constants are α and β, the first one refers to the initial adsorption rate, while the second one is the desorption constant. The interparticle diffusion by Weber and Morris (136) was accomplished following the Equation 4.8.

$$q_t = k_p t^{1/2} \tag{4.8}$$

where t is the time in min and k_p is the constant for the interparticle diffusion equation. It is important to mention that all the fitted data from kinetics models was correlated with the experimental data and validated through the use of the coefficient of determination R^2 (Equation 4.9), root mean square error RMSE (Equation 4.10), and average relative error ARE (Equation 4.11).

$$R^2 = 1 - \frac{\sum_{i=1}^{n}(y_i - \hat{y}_i)^2}{\sum_{i=1}^{n}(y_i - \bar{y})^2} \tag{4.9}$$

$$RMSE = \sqrt{\frac{1}{n-1}\sum_{i=1}^{n}(y_i - \hat{y}_i)^2} \tag{4.10}$$

$$ARE = \frac{1}{n}\sum_{i=1}^{n}\left|\frac{y_i - \hat{y}_i}{y_i}\right| \tag{4.11}$$

4.7 Adsorption equilibrium isotherms

Adsorption equilibrium isotherms were carried out in eight different ways to assure the best fit for the obtained experimental data. All the isothermal parameters were obtained using the Origin® software. Moreover, the models evaluated in this thesis project were Langmuir (99) (Equation 4.12), Freundlich (104) (Equation 4.13), Temkin (137) (Equation 4.14), Sips (138) (Equation 4.15), Liu (139) (Equation 4.16), Dubinin-Radshkevich (140) (Equation 4.17), Redlich-Peterson (141) (Equation 4.18) and Khan (106) (Equation 4.19).

$$q_e = \frac{q_m k_L C_e}{1 + k_L C_e} \tag{4.12}$$

$$q_e = K_F C_e^{1/n_f} \tag{4.13}$$

$$q_e = \frac{RT}{b_T} \ln K_T C_e \tag{4.14}$$

$$q_e = \frac{q_m k_S C_e^{1/n_S}}{1 + k_S C_e^{1/n_S}} \tag{4.15}$$

$$q_e = \frac{q_m (k_l C_e)^{n_l}}{1 + (k_l C_e)^{n_l}} \tag{4.16}$$

$$q_e = q_m \cdot e^{-\beta \epsilon^2} \tag{4.17}$$

$$q_e = \frac{k_{PR} C_e}{1 + a_{PR} C_e^{n_{RP}}} \tag{4.18}$$

$$q_e = \frac{q_m k_K C_e}{(1 + k_K C_e)^{n_K}} \tag{4.19}$$

where, q_m represent the maximum adsorption capacity of the adsorbent in mg/g, all K and n parameters refer to the equilibrium constant (L/mg) and dimensionless exponent from each isotherm, respectively. R indicates the universal gas constant which is 8.314 J/mol·K, T corresponds to the temperature used to carry out the experiments in K, ϵ is the adsorption potential, β shows the mean of sorption free energy and a_{RP} is a second constant from Redlich–Peterson model.

4.8 Adsorption thermodynamic parameters

It is important to establish thermodynamic analysis, which is indispensable to determining the spontaneity and feasibility of the adsorption problem to be faced (142). The thermodynamic behavior of the adsorption experiment presented in this thesis was investigated. Thereby, the Gibbs free energy (ΔG), enthalpy (ΔH), and entropy (ΔS) are calculated using Equations 4.21, 4.22 and 4.20.

$$\Delta G = -RT \ln K_c \tag{4.20}$$

$$\ln K_c = \frac{\Delta S}{R} - \frac{\Delta H}{RT} \tag{4.21}$$

with

$$K_c = \frac{q_e}{C_e} \tag{4.22}$$

where K_c is the distribution coefficient, q_e refers to the amount of BS adsorbed at the equilibrium in mg/g, and C_e is the concentration in mg/L of the concentration remaining on the solution at the equilibrium, respectively. Again, R is the ideal gas constant (which is 8.314 J/mol · K), and T (in Kelvin) is the temperature of the adsorption process of the experiment.

4.9 Regeneration

Using findings from the kinetics, thermodynamics, and isotherm data, the regeneration experiments were adapted. Hence, chemical and solvent regeneration techniques were carried out, using 0.1 g of wasted activated carbon. In this sense, the regeneration processes shown in Table 4.2 below were applied to the waste activated carbon.

Table 4.2: Regeneration methods.

	Reagents	Conditions
1	Methanol	100mL, 60 °C, 24h, constant stirring
2	Ethanol and NaOH (0.5M)	50 mL, proportion 1:1, 5h and room temperature
3	Ethanol and HCl (0.05 M)	50 mL, proportion 1:1, 5h and room temperature
4	HCl (0.1 M)	50 mL, 5h and room temperature

Figure 4.4: Regeneration processes.

After the regeneration process (Figure 4.4), the activated carbon samples were dried overnight and then re-saturated with 100 mL of 200 mg/mL BS. After that, the initial and final concentration of BS was recorder as specified in section 4.2, to be able to calculate the regeneration efficiency (RE). The RE percentage (Equation 4.23) allows comparing the adsorption capacity in both cases: the regenerated and the original.

$$RE(\%) = \frac{q_{reg}}{q_{orig}} \cdot 100 \tag{4.23}$$

where, q_{reg} and q_{orig} are the regenerated adsorption capacity and the original capacity, respectively.

This process was conducted for as many adsorption cycles as the technique allowed. Subsequently, the regenerated carbon samples were characterized to determine the changes due to regeneration, including both the properties that involve surface chemistry, such as textural and compositional ones.

Chapter 5

Results and Discussion

5.1 Macadamia nutshell biomass

Macadamia nutshell precursor was supplied by a local seller from Chihuahua State in 2019. The biomass was dried outdoors in a solar dryer provided by the UNAM Institute of Renewable Energies for two days. The drying step was critical to the subsequent studies. Then the biomass constituents were obtained according to the National Renewable Energy Laboratory (NREL) methodology (46). Data obtained from the macadamia nutshell is shown in Table 5.1.

Table 5.1: Characterization of macadamia nutshell lignocellulosic biomass.

Component	Content (%)
Ashes	5.35 ± 0.03
Extractives	12.57 ± 5.08
Cellulose	50.42 ± 0.48
Hemicellulose	13.75 ± 0.71
Lignin	5.69 ± 0.09

In other work, the same lignocellulosic sample was studied in the production of activated carbon, used for energy storage (143). In addition to the work's main goal, it was determined that the low ash percentage found in macadamia nutshell samples was the primary cause of good carbon production. In other words, a low quantity of inorganic material inside the lignocellulosic matrix will let the organic part be converted into carbon. Additionally, it was found that high cellulose content promotes improvements in the textural properties of the activated carbon surface (144, 145). The analysis of all this information was a determining factor in contemplating the macadamia nutshell as a good alternative to be examined as an adsorbent material.

5.2 Effects of the activation process on the yield and adsorption of BS

Contrary to expectations, ANOVA statistical method found that the activation time and the K_2CO_3:precursor molar ratio were not significant based on their p-values. For this analysis, it was stipulated an α value of 0.05 which was lower than those obtained for time and impregnation ratios factors (0.546 and 0.466, respectively). On the other hand, the activation temperature showed a high degree of significance in the prediction of the model, resulting in a p-value of 0.009. In other words, the activation temperature had a significant contribution on the yield of activated carbon and BS adsorption, which could also be confirmed with equations 5.1 and 5.2.

From the regression equations, the positive coefficients denote proportionality between the independent and dependent variables, and the negative ones otherwise. That is, when the factor increases in level, the response variable for positive coefficients also increases. For this reason, it has been observed that temperature has an important impact on the activated carbon final mass because yield increases at low temperatures. Which means that the relationship between temperature and yield is inverse. Equation 5.1 and 5.2 represents the regression equation of the yield and BS adsorption, respectively.

$$\begin{aligned} Yield = 25.33 + 0.633x_1 - 3.663x_2 + 0.302x_3 - 0.67x_1^2 \\ -1.03x_2^2 + 0.02x_3^2 + 1.75x_1x_2 - 0.91x_1x_3 + 1.15x_2x_3 \end{aligned} \tag{5.1}$$

$$\begin{aligned} BSads = 82.94 + 3.14x_1 + 16.38x_2 + 2.58x_3 + 5.03x_1^2 \\ -15.11x_2^2 - 11.27x_3^2 - 4.73x_1x_2 - 3.16x_1x_3 - 4.34x_2x_3 \end{aligned} \tag{5.2}$$

In evaluating the factor interactions over the response variables, temperature-K_2CO_3-precursor molar ratio interaction was the most important interaction that influences on the BS adsorption. In accordance with Table 5.2, the range of activated carbon yield found for these experiments was from 16.47% (Run 8) to 28.08% (Run 3). For the BS adsorption response variable, the results ranged from 30.7% (Run 1) to 86.5% (Run 2). Additionally, it was found that the central points from the experimental design (Runs 13, 14, and 15) have a standard deviation of 1.081 for yield factor and 1.07 for BS adsorption. This correlation could be interpreted as good consistency and reproducibility in the performance of the experiments.

Results from this section were important for selecting the best sample based on its performance to carry out the adsorption experiments. Therefore, Run 2 was selected according to its low activating agent usage, moderate activation temperature and time, and good performance on the response variables evaluated. It is important to highlight that because time and K_2CO_3:precursor factors have less influence on the response vari-

ables of the model, it is not necessary to employ more resources, which could increase material and operational costs.

Table 5.2: Extended Box–Behnken design matrix for K_2CO_3 chemical activation and the influence of factors over BS removal and yield.

Run	IR (x_1)	Temp. (x_2)	Time(x_3)	Yield (%)	BS removal (%)
1	2:1	700	1	27.39	30.70
2	2:1	900	1	18.26	86.50
3	2:1	700	2	28.08	35.30
4	2:1	900	2	23.56	86.32
5	1:1	700	1.5	27.80	58.24
6	3:1	900	1.5	22.97	78.00
7	3:1	700	1.5	27.30	69.07
8	1:1	900	1.5	16.47	86.10
9	1:1	800	1	24.90	60.74
10	3:1	800	2	22.64	73.74
11	3:1	800	1	26.26	78.26
12	1:1	800	2	24.94	81.46
13	2:1	800	1.5	25.16	83.64
14	2:1	800	1.5	26.48	81.71
15	2:1	800	1.5	24.34	83.47

Note: IR, impregnation ratio and Temp, temperature

5.3 Characterization of activated carbon samples

The best two samples (Run 2 and 4) and those that displayed less efficiency in the variables assessed (Run 1 and 3) in the previous section were subjected to the characterization process. The objective was to describe the properties that make certain behaviors possible for the response variables. Thus, the chemical composition of the samples was determined through EDS analysis. The samples contain mainly carbon, followed by oxygen, nitrogen, silica, and potassium. Table 5.3 show the exact percent-

ages of the elements.

Table 5.3: Chemical composition of the samples

	Carbon (%)	Oxygen (%)	Nitrogen (%)	Silica (%)	Potassium (%)
Run 1	82.65	11.96	5.05	0.37	-
Run 2	85.55	7.78	3.20	2.18	1.29
Run 3	62.00	30.70	4.14	3.16	-
Run 4	78.13	12.67	3.00	3.90	2.30

Evidently, according to Table 5.3, Run 2 has the highest percentage of carbon than the rest of the samples. The impurities of Si could be a result from the intrinsic composition of macadamia nutshell biomass (33, 146). Also, the best samples Run 2 and 4 contains potassium. The common characteristics between these two samples were temperature (900 °C) and the concentration of activating agent (ratio 2:1). This means that the activating agent probably reacts differently at high temperatures, so small amounts of potassium appear on the activated carbon structure that were perhaps crystallized in the activated carbon structure.

The micrographs of the samples at different magnifications were obtained from SEM equipment (Figure 5.1). The 1500x micrographs shows the porosity distribution throughout the samples surface. Figures 5.1b and 5.1c, shows the non-homogeneous distribution of porosity of the activated carbon samples. The white deposits on the surface are inorganic elements of silica, and potassium as indicated in the EDX analysis.

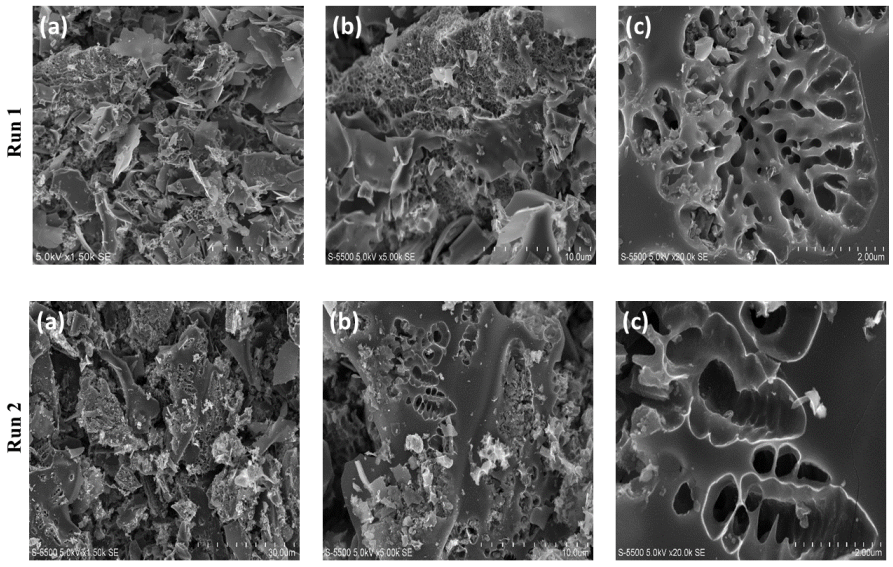

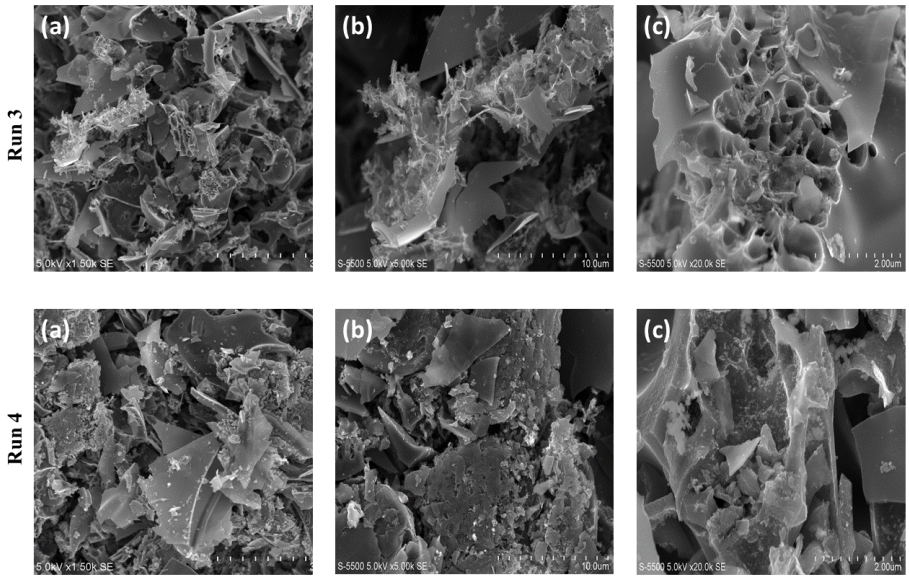

Figure 5.1: Micrographs from SEM at: (a) 1500x, (b) 5000x and (c) 20000x magnifications.

The FTIR analysis was carried out to determine the functional groups on the activated carbon samples. Figure 5.2 shows that the four samples evaluated have a similar signal at ∼3430 cm^{-1}, which represents the band due to combined vibration of amine functional group (N-H) and hydroxyl groups (O-H) (147). These last ones are due to proton vibrations occurring in water molecules. Thus, the vibrations at ∼2345 cm^{-1} are assigned to C≡C functional group , which describes the intrinsic properties of activated carbon (146, 148). Also, the samples show an intense response at ∼1560 cm^{-1}, which is identified as carbonyl functional group (C=O), and can be attributed to the stretching of aromatic ring of the carbon (149). The peaks at ∼1107 cm^{-1} and ∼814 cm^{-1} are due to C-O bonding, typically assigned to ether alcohol and ether group (150, 151).

However, for Run 1 and Run 3 at frequencies ∼1107 cm^{-1}, the peaks vibrate slightly out-of-phase compared to the best samples (Run 2 and Run 4). The mentioned delay is caused by the displacement of the central atom of the functional group (152). In this case, the mentioned out-of-phase vibration could affect the interaction between the surface chemistry and pollutants of BS. A high concentration of these functional groups could influence the adsorption processes because of the hydrogen bonds formed between the water and oxygenated functional groups, which block the access of pollutants to the porosity of activated carbon (153).

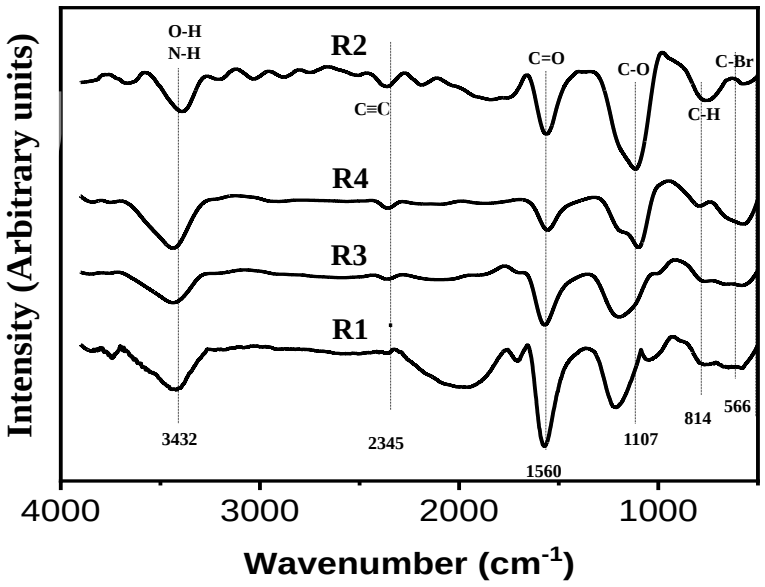

Figure 5.2: FTIR spectra for macadamia nutshell activated carbon samples.

The physisorption isotherms were obtained from the four samples evaluated under N_2 atmosphere. All the data obtained from this characterization technique are shown in Table 5.4. As expected, Run 1 and 3 were the samples that showed the lowest surface area in both analysis methods of BET and DFT. Thus, the surface area of Run 4 was found to be slightly higher than Run 2; however, the pore volume of Run 2 is larger than that of Run 4. According to the literature, if the pore volume is increased, it can promote the adsorption of contaminants with larger particle sizes and, at the same time, prevent pore clogging (154). Also, it could be noted that the affinity of Run 2 over the rest of the samples to adsorb the binary solution is mainly related to the chemical characteristics of the adsorbent surface and the pore volume.

Table 5.4: Data obtained from physisorption isotherms.

Sample	BET surface (m^2/g)	DFT surface (m^2/g)	Pore volume (cc/g)	Half pore width (nm)
Run 1	547.38	727.18	0.38	0.33
Run 2	1225.41	1239.70	0.80	0.46
Run 3	661.51	763.06	0.40	0.46
Run 4	1272.60	1280.66	0.75	0.50

Figure 5.3a displays the isotherm shape of each of these four samples. Clearly, all the isotherms shows a combination of Type I and IV accompanied by an adsorption-desorption hysteresis of Type H4 according to IUPAC nomenclature (155). This type of isotherm is mainly due to the presence of micro and mesopores. Also, Figure 5.3b shows two peaks, which correspond mainly to mesopores, with a small contribution of micropores, confirming the isotherm trend.

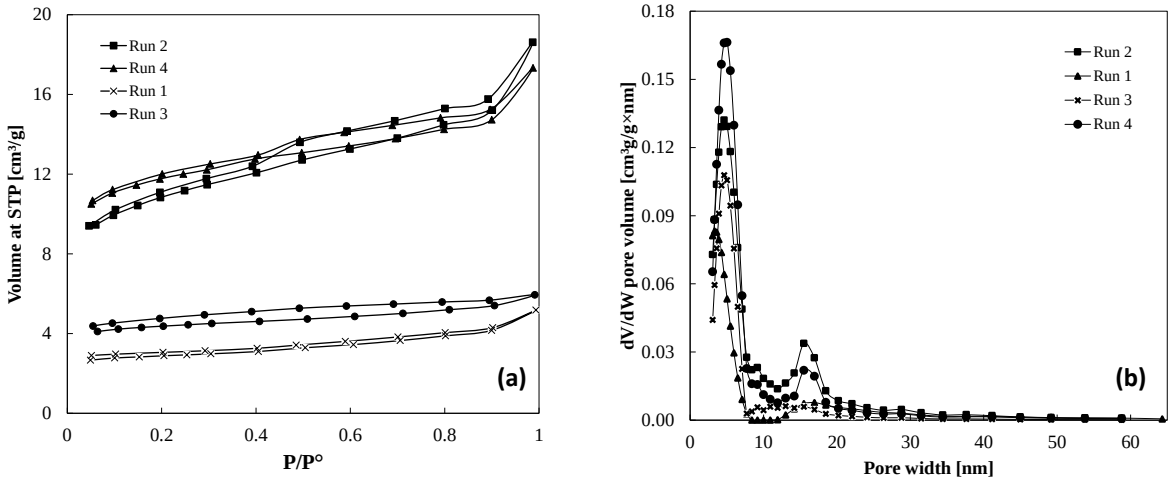

Figure 5.3: (a) Adsorption–desorption isotherm, and (b) pore size distribution following DFT methodology.

5.4 Effect of pH and determination of pHpzc

As mentioned above, Run 2 was selected for the adsorption experiments. The pH has a significant impact on the adsorption mechanism since it controls the charges on the adsorbent surface and influences the degree of ionization of the solution components (12). Figure 5.4a shows the effect of pH for BS adsorption experiments in a pH range of 2 to 12. The results shown in this graph indicate that the activated carbon sample evaluated could function in a wide range of pH values. However, there is a considerable decline in pollutants removal in strong alkali environment. The best adsorption was obtained at pH 6, reaching a 87.4% of BS adsorption (75.85% of AMX and 99.98% of MB removal). On the other hand, lowest behaviour was obtained from pH 10 and 12, with 82.0% and 73.5% of BS removal, respectively. Based on what has been previously described, neutral pH has been selected as the appropriate one to handle the rest of the experiments.

Besides, the pHpzc is the point when the surface charge on the activated carbon is neutral, knowing its value could helps to measure the electrokinetic conditions of the evaluated materials (156). For Run 2, the pHpzc is 4.5, indicating an acidic behaviour

of this sample (Figure 5.4b). Therefore, at pH higher than pHpzc (pH>4.5), the surface of Run 2 is negatively charged and could adsorb cations contained in BS, in this case, the MB (157, 158). Likewise, when the pH is lower than 4.5 (pH<4.5), the anionic substances develop a better affinity with the adsorbent, which is positively charged. In other words, in this scenario AMX would preferentially adsorb on the carbon surface.

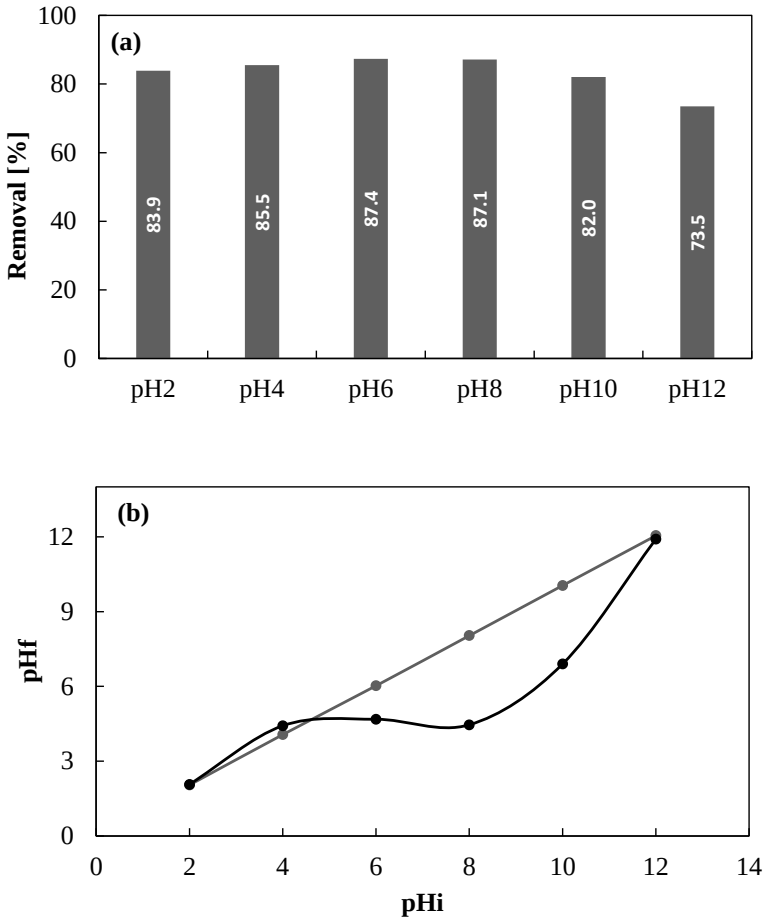

Figure 5.4: Effect of pH in adsorption of BS. (a) Percentage of binary solution removed at different pH values, and (b) determination of pHpzc for Run 2 in BS.

Figure 5.5 indicates the removal percentage of each pollutant contained in the BS solution at different pH values. In the pH range evaluated, there are no changes for MB removal percentage, which suggests that the forces involved here are mostly $\pi - \pi$ interaction (159, 160). The above indicates that AMX has a synergistic behaviour towards MB, hence, it is not affected by the presence of AMX (161).

On the other hand, it was expected that AMX would have a better adsorption ca-

pacity at acidic pH; however, the optimal pH for AMX removal in BS was close to neutral pH, that is ∼6 (75.85%). Under acidic conditions are predominantly negative ions (with –COOH already converted to –COO–) and the surface of Run 2 is positively charged (pH< 4.5), therefore, the predominant adsorption mechanism is mainly through electrostatic forces (162). When the pH was increased, the surface of Run 2 activated carbon sample becomes negatively charged (pH>4.5), which causes electrostatic repulsion of mentioned anions, and initiates a competition adsorption process between the OH– groups from the alkalinity of the solution and –COO– functional groups from AMX (163).

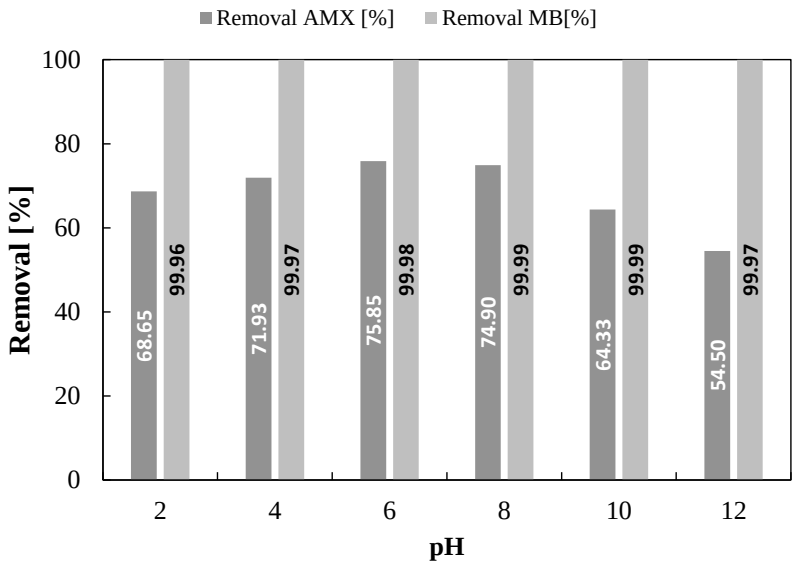

Figure 5.5: Removal of each pollutant from BS at the corresponding pH.

5.5 Effect of activated carbon concentration

Different concentration of activated carbon using Run 2 sample were tested to investigate its effect on the adsorption process. To achieve this objective, various experiments were prepared, with 0.1 g, 0.15 g, 0.2 g, 0.25 g, and 0.3 g amounts of activated carbons. Then, 100 mL of 400 mg/L of BS was added to each experiment at neutral pH during the next 24 h.

From the results displayed on Figure 5.6, it was observed that the removal capacity of BS increases as the dosage of Run 2 sample was increased. About 100% of MB removal and 98.6% for AMX was realized at 0.3 g concentration of the activated carbon. The percentage adsorption of MB was higher than AMX over the entire range of acti-

vated carbon concentrations tested, probably due to the difference of charges present on the surface of the activated carbon and the ions of the BS, which was discussed in a previous section. In other words, the competitive adsorption between these two BS components allows MB to be adsorbed first due to its affinity with the activated carbon sample, and then AMX could be available to be adsorb in the remaining active sites (164). This phenomena occurs principally on the micropore region (165), which is characterized by being the main one that has the largest number of active sites for adsorption in aqueous solutions mechanism (166).

Therefore, only the AMX adsorption was proportional to concentration of Run 2. Considering the results and associated costs in producing activated carbon, a dosage of 0.2 g was selected to carry out the rest of the experiments. This adsorbent concentration shows an adequate adsorption capacity without the need for large quantity of activated carbon.

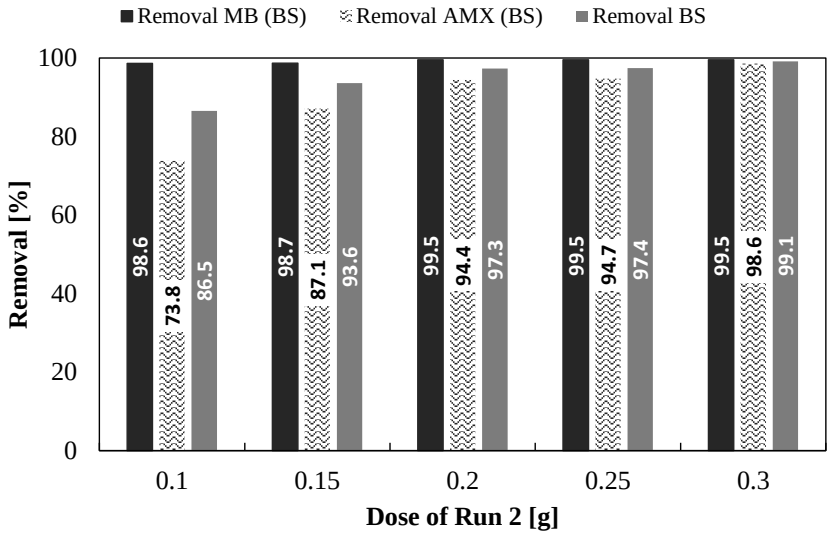

Figure 5.6: Effect of activated carbon concentration on adsorption processes at 150 rpm for 12 h and room temperature.

5.6 Effect of temperature

The influence of temperature was investigated at 30 °C, 40 °C, and 50 °C. Parameters such as pH and adsorbate dosage were maintained under the optimal conditions already selected in previous sections, that is, 0.2 g of Run 2 activated carbon and neutral pH. The contaminated solution used for these experiments was at its maximum concentration of 800 mg/L BS. Usually, an increase in temperature is expected to promote adsorption mechanisms (82). This is because as increasing temperature, decreases the

viscosity and increases molecular motion allowing the pollutants to be adsorbed on the activated carbon.

Figure 5.7 indicate that above 40 °C, the equilibrium adsorption was slightly decreases, approximately by 10 mg/g. Further increase in temperature above 50 °C will promote the reversibility of the adsorption equilibrium (119). From the viewpoint of the input energy and resources employed, a temperature of 40 °C was selected as the optimal temperature for this material and adsorbate.

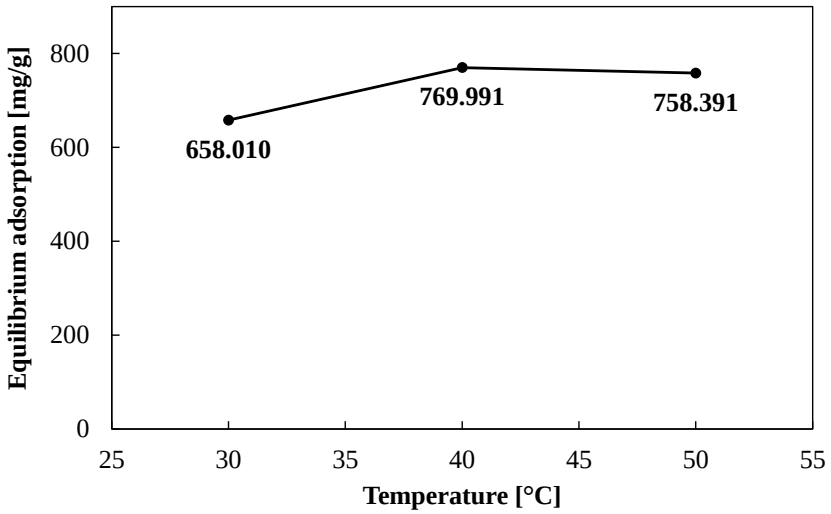

Figure 5.7: Effect of temperature for BS adsorption with Run 2 probed at 30, 40 and 50 °C, for 24 h and 150 rpm.

5.7 Effect of contact time and kinetic of adsorption

An adequate contact time ensures that the adsorbent achieve the adsorption equilibrium. This analysis promotes the understanding about the behavior of the adsorption rate as a function of temperature and BS concentration. The experiments described in this section were carried out using different concentrations of BS (50, 100, 200, 400, 600, and 800 mg/L), always maintaining the same proportion of AMX and MB in each experiment. That is to say, for instance, a concentration of 50 mg/L of BS solution was prepared by adding 25 mg/L MB and 25 mg/L AMX. Thus, neutral pH was used, with temperatures of 30 °C, 40 °C, and 50 °C. The experiments were extended until no changes were found in the BS concentration in each of the tests evaluated.

In this context, Figure 5.8 shows that for all temperatures employed, BS adsorption

increases with time until equilibrium is reached. For all the experiments, it could be observed that there is strong adsorption in the first 15 minutes, followed by slower adsorption. In this sense, for the lowest BS concentrations (50, 100, and 200 mg/L), it was observed that the temperature does not represent a factor that significantly affects the adsorption process, due to the abundance of active sites available to adsorb the BS components. In experiments with a BS concentration of 50 and 100 mg/L, equilibrium was practically reached in the first two minutes. When the concentration increased from 400 mg/L to 800 mg/L, equilibrium was obtained from 400 min onwards. The adsorption speed accomplished in these experiments could be interpreted as a strongly initial adsorption, propagated by the free active sites on the surface of Run 2.

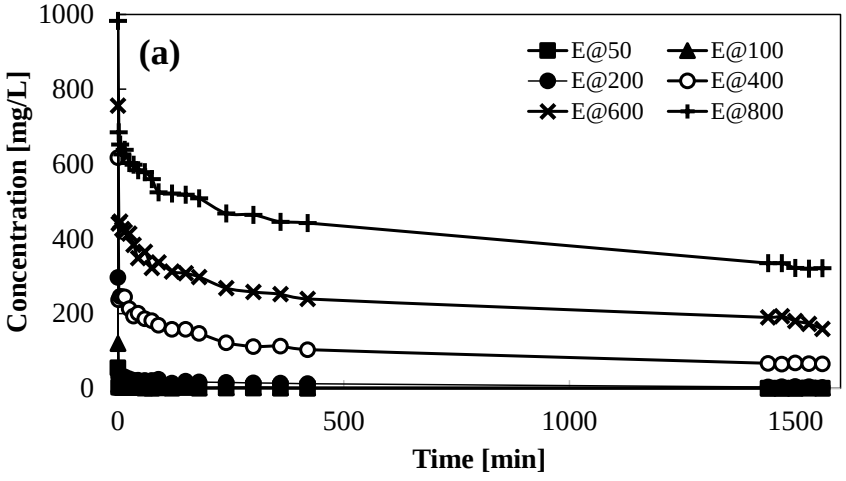

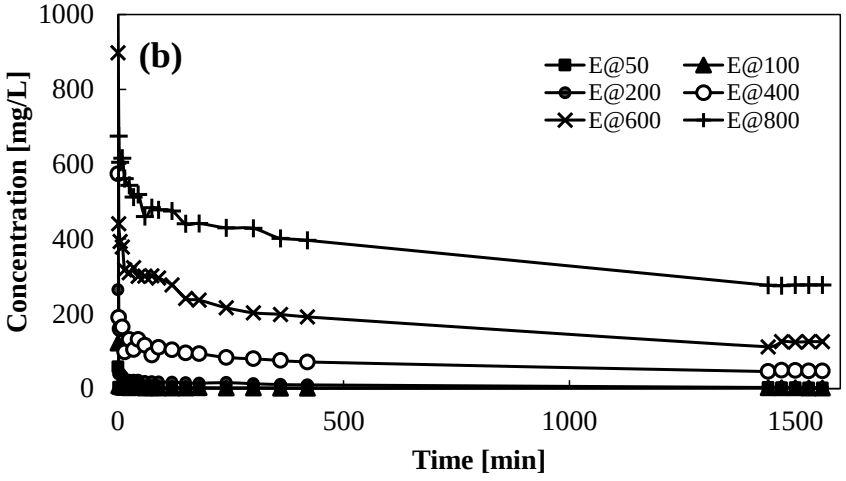

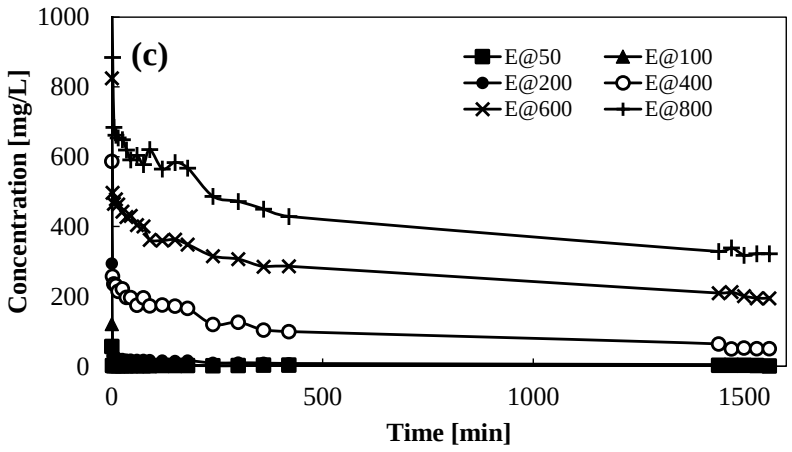

Figure 5.8: Effect of contact time in the removal of BS using 0.2 g of Run 2, neutral pH at (a) 30 °C, (b) 40 °C and (c) 50 °C.

Moreover, the intraparticle diffusion study was carried out with the objective of describing the adsorption rate and mass transfer mechanisms that govern the samples already mentioned. Thereby, Weber and Morris (136) methodology was applied. This model suggests multi-linearity a result of plotting q_t (the amount of BS adsorbed at one time in mg/g) versus $\sqrt{t}$. Consequently, each segment of slope found on the graph represents a different mass transfer stage within the adsorption mechanism.

Figure 5.9, is a clear example of the aforementioned multi-linearity, where the points are the experimental data obtained plotted with respect to $\sqrt{t}$. Evidently, two segments were found. The first segment refers to the mass transfer (BS) process on the external surface of the carbon sample (instantaneous adsorption); the second slope is attributed to a gradual adsorption governed by the intraparticle diffusion uptake rate (32, 167, 168). As shown in Table 5.5, for the series of experiments conducted in this section, most of the segmentations found were two for each case, so the interpretations are similar to Figure 5.9. However, some cases were recorded where three slopes were appropriate to describe the behavior of those experiments. In this case, the third slope has to do with the equilibrium caused by the decrease in the concentration of the adsorbate (BS) (169).

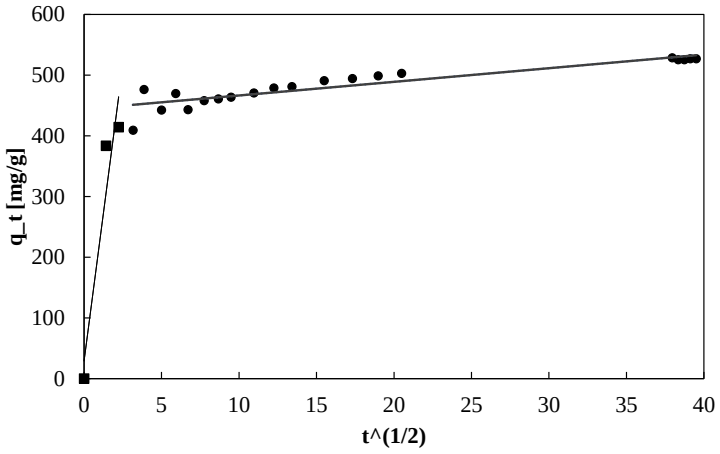

Figure 5.9: Weber and Morris intraparticle diffusion model analysis. Experiment carried out at optimal conditions: Neutral pH, 0.2 g of Run 2 sample, 40 °C and 400 mg/L of BS.

Some authors indicate that the values of C_i could provide information about the thickness of the boundary layer. Therefore, if the value of the intersection (C_i) is large, the effect on the boundary layer of the adsorption process also increases. In other words, a positive value of C_i suggest that the adsorption is affected by some mechanism other than the process of internal diffusion (170). C_i values are shown on Table 5.5 in the Appendix, Section A.2.

On the other hand, initial adsorption factor (R_i) was obtained from each concentration at different temperatures (Table 5.5), using the same method. For this case, it was found that experiments using from 50 mg/L to 600 mg/L of BS result in a strongly initial adsorption (R_i value between 0.5 and 0.1). Meanwhile, for the experiment using at 800 mg/L, it was found to have an R_i value between 0.9 and 0.5, which means an immediately initial adsorption behavior (171). The exception was for the experiment carried out at 40 °C and 800 mg/L, for which it was obtained strongly initial adsorption.

Table 5.5: Interparticle diffusion initial adsorption behavior analysis.

	30 °C		40 °C		50 °C	
Exp	Initial adsorption factor (Ri)	Adsorption behaviour	Initial adsorption factor (Ri)	Adsorption behaviour	Initial adsorption factor (Ri)	Adsorption behaviour
E@50	0.128	3	0.120	3	0.111	3
E@100	0.340	3	0.115	3	0.132	3
E@200	0.181	3	0.352	3	0.238	3
E@400	0.400	3	0.270	3	0.465	3
E@600	0.468	3	0.384	3	0.544	2
E@800	0.536	2	0.462	3	0.576	2

Strongly initial adsorption (3), intermediately initial adsorption (2), according to (171).

Additionally, the experimental kinetic data obtained at different BS concentrations and temperatures (that is, 30 °C, 40 °C, 50 °C) were fitted with pseudo-first order kinetic (PFO), pseudo-second order kinetic (PSO), and Elovich models. The results of the fitting are shown in Figure 5.10, 5.11, and 5.12. Observably, from the fitting obtained at 30 °C (Figure 5.10 and Table A.2), PSO and, consequently, Elovich were the models that best fit the data at this temperature. This could be validated according to the range of coefficients of determination (R^2), the error analysis based on root-mean-square error (RMSE), and the absolute relative error (ARE).

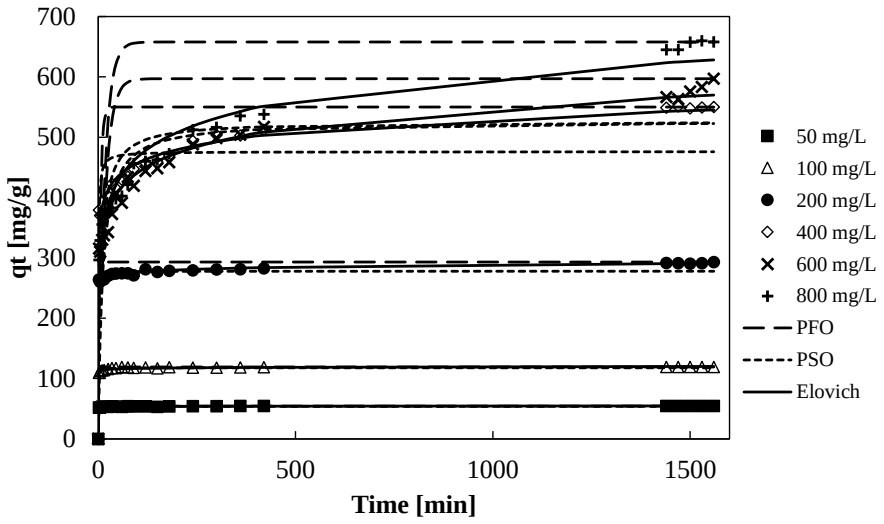

Figure 5.10: PFO, PSO and Elovich kinetics modelling fitted to experimental data from different initial concentration at 30 °C and neutral pH.

From the PFO, R^2 was obtained in the range located at 0.999–0.913, an RMSE value of 0.84–147.58, and a range of 0.011–0.249 for ARE. The PSO, for its part, presented R^2, RMSE, and ARE ranges of 0.999-0.927, 0.537-81.80, 0.008-0.138, respectively. Whereas, Elovich model have R^2 of 0.999-0.985, RMSE of 0.371-25.551, and ARE of 0.005-0.051. This information suggests that the interaction mechanism between the activated carbon Run 2 sample and the BS is mainly via chemisorption, according with the good PSO and Elovich fitting. Besides, the adequate adaptation of the Elovich model to the kinetic data with very low error and high R^2 indicates heterogeneous adsorption on the surface of the Run 2 sample (85, 86, 90).

On the other hand, Table A.3 and Figure 5.11 indicate that the pseudo second order and Elovich models fit the experimental data well, according to the values of R^2, RMSE and ARE. As explained above, this means that the mechanism that governed the adsorption process at 40 °C was mainly chemisorption.

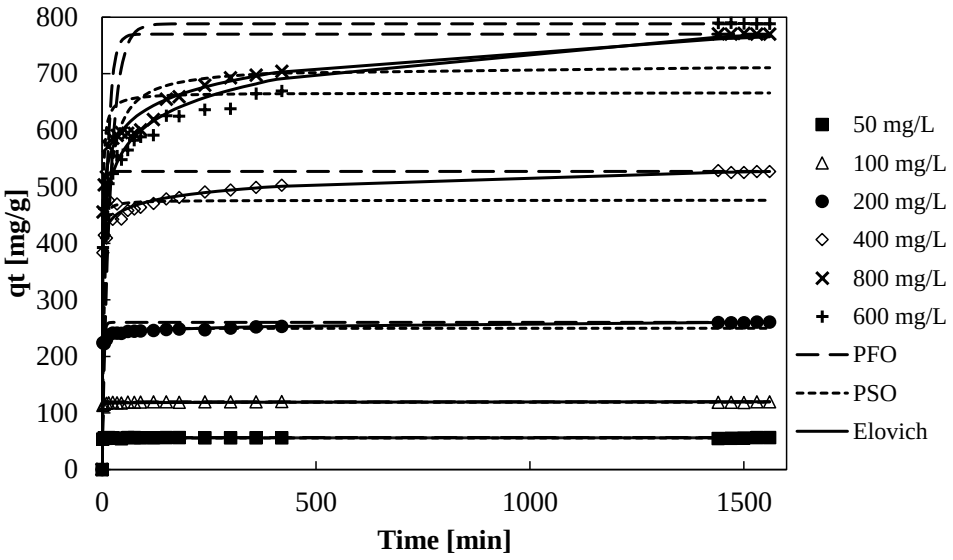

Figure 5.11: PFO, PSO and Elovich kinetics modelling fitted to experimental data from different initial concentration at 40 °C and neutral pH.

Similarly, the data shown in Table A.4 and Figure 5.12 demonstrated a good relationship between experimental data and the pseudo-second order model, and therefore to the Elovich model.

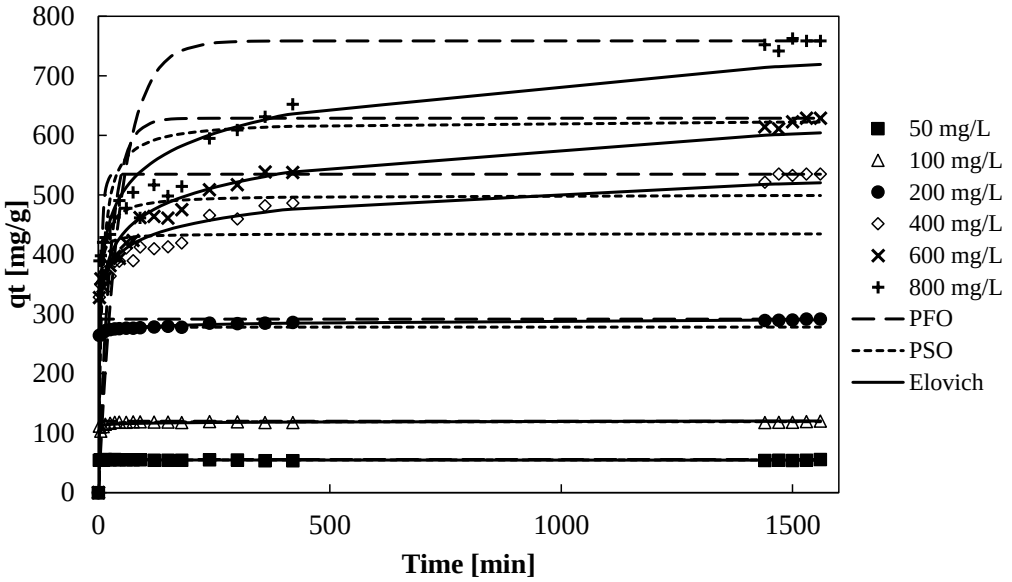

Figure 5.12: PFO, PSO and Elovich kinetics modelling fitted to experimental data from different initial concentration at 50 °C and neutral pH.

In general, all kinetics experiments at their smallest concentrations showed a good fit with respect to the kinetic models of PFO, PSO, and Elovich. The above completely rules out the effect of temperature on them. On the contrary, in experiments that were carried out at concentrations higher than 200 mg/L, the error values increased considerably. Despite the values obtained for the errors, the main adsorption mechanism was chemisorption. It should be noted that PSO is an adequate model for low-concentration solutions, which may be the main reason that PSO has not adapted exactly to high concentrations (92). However, the good fit with the Elovich model confirms the speculations about the adsorption mechanism involved in BS and Run 2, which is chemisorption.

5.8 Isotherm modelling

The interaction mechanism between Run 2 and BS could also be described by adsorption isotherm models by obtaining information on values such as maximum adsorption capacity, energy, and surface properties, among others (80). In this sense, eight isotherm models were evaluated for this project, and all the data obtained were correlated and validated by R^2. Table 5.6 contains the data from the best isotherm fitting; the rest of the models are shown on Table A.5 in the Appendix, Section A.

Table 5.6: Data obtained from several isotherm models at different temperatures.

	303 K	313 K	323 K
Sips			
K_s	0.221	0.117	0.195
n_s	0.608	1.601	1.755
q_m	603.201	1016.144	848.560
R^2	0.979	0.966	0.961
Temkin			
B_i	93.955	132.160	85.112
K_T	4.166	1.701	45.496
R^2	0.968	0.972	0.964
Khan			
q_m	467.926	386.2639	349.2194
K_K	0.39745	0.31641	0.5623
n_K	0.93297	0.833114	0.85935
R^2	0.978	0.967	0.975

The fitting adjustment curves are shown in Figure 5.13. It was found that the best fit was the Khan isotherm, according to the value of R^2, which is close to unity. Furthermore, the Khan isotherm model is a hybrid of the Langmuir and Temkin isotherms that has been developed specifically for pure substance adsorption (bi-adsorbate adsorption), which correspond with the phenomenon described by Majd et al. (102). The Sips isotherm model, which is a hybrid of the Langmuir and Temkin isotherms, also presented a good fit to the experimental data. As expected, the Temkin isotherm is also appropriate for describing the adsorption phenomenon described in this thesis. At higher concentrations, Sips isotherms highlight heterogeneous adsorption systems governed primarily by monolayer behavior (97), which refers again to chemisorption.

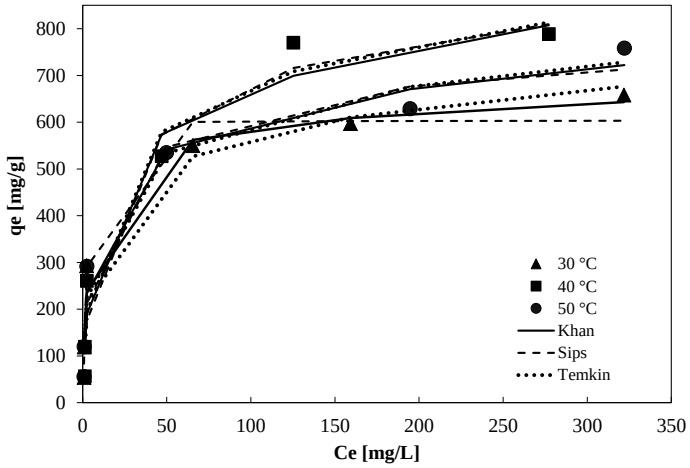

Figure 5.13: Experimental data of adsorption isotherm and their fitting of Sips, Temkin and Khan isotherm models at different temperatures.

Besides, separation factor (R_L) from Langmuir isotherm was evaluated at different temperatures and initial BS concentrations to study the nature of the adsorption process and to describe the affinity of BS molecules to Run 2 surface (Figure 5.14). R_L values obtained were between 0 and 1, these values exponentially decrease as the initial concentration increases, indicating a favourable adsorption (98). In addition, the adsorption intensity values ($1/n_F$) obtained in this work were less than zero in all temperatures, which indicates that the adsorption processes are favourable (100).

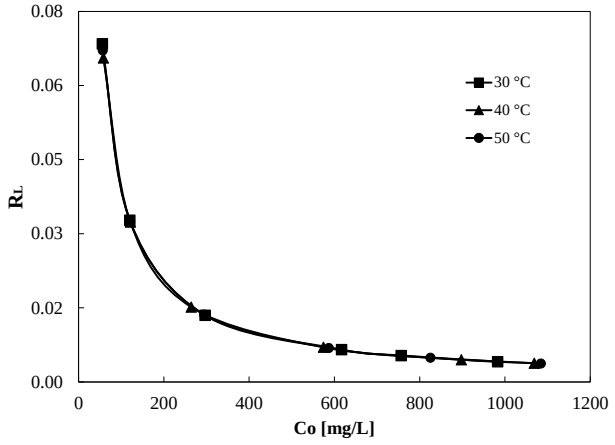

Figure 5.14: Separation factor evaluated at different temperatures.

5.9 Adsorption thermodynamics

The Gibb's free energy (ΔG), enthalpy (ΔH), and entropy (ΔS) thermodynamics parameters were calculated for the experimental data obtained. These thermodynamic values could give an idea of the spontaneous or non-spontaneous nature of the adsorption and the feasibility of the adsorption process (89). The ΔS and ΔH parameters were obtained by the Van't Hoff equation resulting from using Equation 4.21. This equation provides specific values of slope and intercept, which are related to ΔH and ΔS, respectively. The graph obtained from these calculations is shown below (Figure 5.15).

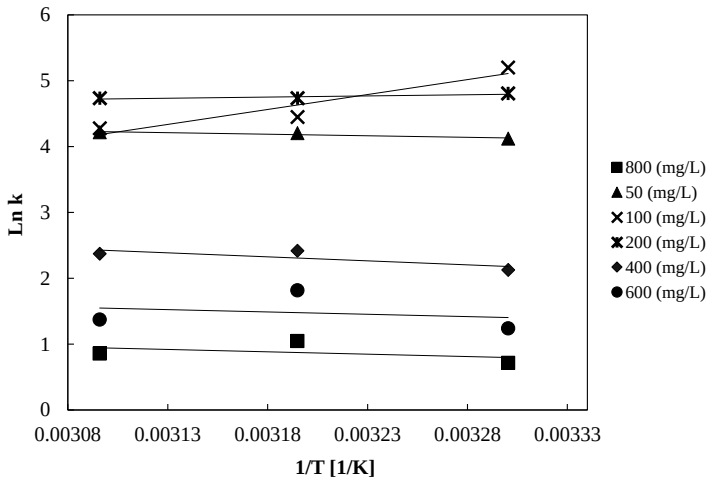

Figure 5.15: Curves obtained from Van't Hoff equation at each concentration.

The specific values calculated to each curves were register on Table 5.7. For the Gibbs free energy of change (ΔG), only negative values were found, which according to the literature means that the process was feasible and that it occurred spontaneously (142). Analyzing the results obtained from enthalpy, negative values were found for the experiments carried out at low concentrations (100 and 200 mg/L), which totally describes an adsorption of an exothermic nature. Likewise, the experiments with positive ΔH describe adsorption processes of endothermic origin (172). Additionally, this parameter is closely related to the activation energy (E_a) according to the Arrhenius equation and therefore the calculation of the variables involved is similar. In simple terms, $E_a \sim \Delta H$ (173).

As occurred in the case of ΔH, negative values of ΔS were also obtained for one experiment with the lowest initial concentration (100 mg/L). This suggests that this process is clearly governed by enthalpy, due to the decreased disorder of the process. Positive ΔS, for its part, indicates high affinity between the adsorbent and the adsorbate (BS)

(34).

Table 5.7: Thermodynamics parameters of the adsorption process.

Experiment	ΔG (KJ/mol)			ΔH (KJ/mol)	ΔS (J/mol)
	303 K	313 K	323 K		
E@50	-10.38	-10.94	-11.32	3.94	47.35
E@100	-13.10	-11.58	-11.49	-37.72	-82.01
E@200	-12.11	-12.32	-12.72	-2.92	30.22
E@400	-5.36	-6.29	-6.37	10.10	51.45
E@600	-3.12	-4.72	-3.69	5.88	31.07
E@800	-1.80	-2.72	-2.30	5.96	26.31

5.10 Regeneration

The results from each regeneration method implemented are shown on Table 5.8. In this sense, after 4 cycles of regeneration, the best regeneration method based on the removal capacity was the one elaborated with a mixture of ethanol and sodium hydroxide, obtaining a BS removal of 42.57% and a RE percentage of 41.14. From this methodology it was found that MB was the compound that showed a better response to the removing substances, reaching even a 0.98 mg/L as final concentration of MB (Figure 5.16). Also, it can be shown how the adsorption capacity decreased with respect to the number of saturations carried out.

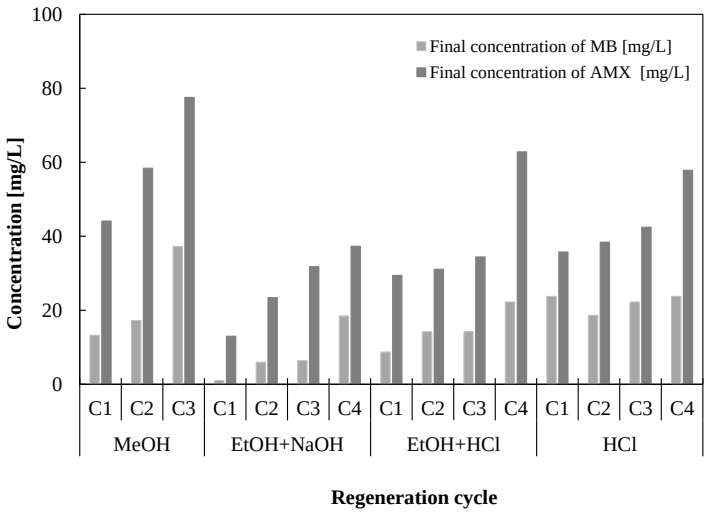

Figure 5.16: BS components remaining of each regeneration technique.

In this regard, the reaction resulting from the mixture of ethanol and NaOH is shown in Equation 5.3, which contains a proportional amount of ethoxyl and hydroxyl ions (174).

$$CH_3CH_2OH + NaOH \longrightarrow CH_3CH_2O^-Na^+ + H_2O \tag{5.3}$$

As can be seen, these ions are characterized by being a strong base. Both ions, when interacting with the surface of the adsorbent, and in particular the ions coming from the BS contaminants, facilitate the removal of contaminants from the adsorbent. Hence, it can be concluded that the percentage removal of MB is higher than that of AMX for this regeneration experiment: the S^+ cation of MB interacts more easily with the hydroxyl (OH^-) and ethoxide ($CH_3CH_2O^-$) ions present in the regeneration solution (175).

Table 5.8: Results of each regeneration method through the cycles performed.

	Removal BS (%)	RE (%)
MeOH		
C1	76.35	71.84
C2	58.13	26.46
C3	29.71	15.07
EtOH+NaOH		
C1	83.47	80.71
C2	75.86	73.33
C3	64.76	62.63
C4	42.57	41.14
EtOH+HCl		
C1	54.87	28.80
C2	41.62	13.94
C3	52.94	12.71
C4	48.24	10.42
HCl		
C1	72.42	68.13
C2	67.54	52.45
C3	31.45	32.77
C4	26.12	20.96

On the other hand, a small amount of AMX compound remains on the adsorbent surface after being regenerated, in some cases its concentration exceeded 80%. This phenomena could occur due to the low affinity to the characteristic carboxylate anion ($RCOO^-$) of amoxicillin and other β-lactam antibiotics (176, 177), which is caused by the dissociation of carboxylic acids. Generally it was found that the regeneration methods developed with methanol and hydrochloric acid yielded lower removal efficiency and

RE percentage.

The characterization of the regenerated adsorbents was carried out after the fifth regeneration process. Table 5.9 shows the information collected from the physisorption studies. As can be seen, the regeneration method based on a mixture of ethanol and NaOH, despite being the most effective in removing the BS solution from the surface of the adsorbent, was nevertheless the one that had the greatest effects on the morphology of the activated carbon.

Table 5.9: Comparative table on the porosity of the regenerated carbons and the original Run 2 sample.

After fifth regeneration	Run 2	Reg. MeOH	Reg. EtOH+NaOH	Reg. EtOH+HCl	Reg. HCl
BET surface area (m^2/g)	1225.4	70.1	0.00	2.5	62.8
DFT surface area (m^2/g)	1239.7	87.6	28.0	115.4	112.6
Pore volume ($cm\hat{3}/g$)	0.8	0.2	0.07	0.2	0.2
Half pore width (A)	4.6	16.9	22.1	15.5	15.5

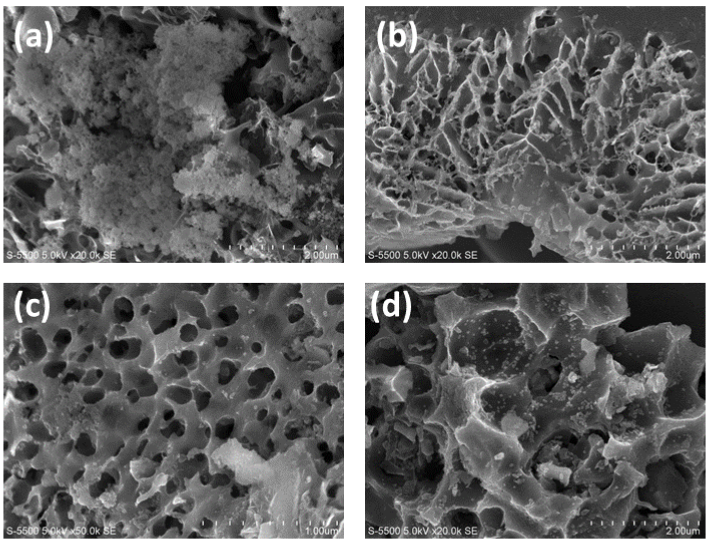

Figure 5.17: Micrographs from SEM at 20000x magnifications for: (a) Reg. EtOH+NaOH, (b) Reg. HCl, (c) Reg. EtOH+HCl, and (d) Reg. MeOH.

However, Figure 5.17 shows the SEM micrographs obtained for the activated carbon samples subjected to the regeneration methods already mentioned. In this sense, in Figure 5.17a. it could be easily seen that for the experiment carried out with ethanol

and NaOH, it has a dirty surface. This suggests that the change in morphology of the activated carbon sample is mainly because of the contaminants sticking on the surface of the carbon.

The EDS composition analysis (Table 5.10) showed that some different elements were added to those contained in Run 2. These elements were sodium, sulfur, and aluminum, which may be traces in the NaOH-based solution, and the sulfur contained in both MB and AMX.

Table 5.10: Comparative table on the porosity of the regenerated carbons and the original Run 2 sample.

	C (%)	O (%)	N (%)	S (%)	Si (%)	Na (%)	K (%)	Cl (%)
MeOH	78.98	9.87	7.36	3.16	0.63	-	-	-
EtOH+NaOH	76.78	10.51	5.06	5.22	1.08	0.98	-	-
EtOH+HCl	78.93	11.19	7.07	2.43	0.39	-	-	-
HCl	80.04	10.41	-	1.76	5.05	-	1.71	1.03

As the last step, FTIR studies were carried out on the four activated carbon samples subjected to the different regeneration processes. The functional groups found could be seen in Figure 5.18. The signal at ∼3736 cm^{-1} was attributed to (O−H) vibrations in hydroxyl groups (178, 179) and the vibrations at ∼3380 cm^{-1} are assigned to the amide group (N−H) (180). Both functional groups were merged into the original Series 2 sample; however, in the regenerated activated carbon samples, a displacement of both functional groups was obtained.

Thus, the peaks presented at ∼1740 cm^{-1} is due by ester carbonyl group C=O (154). The signals found at ∼1310 cm^{-1} (181, 182) and ∼814 cm^{-1} (183, 184) are caused by methylene (C−H) stretching, the second peak of this functional group was the only one different from those found in the original Run 2 sample. The possible cause of this finding is the addition of new functional groups characteristic of the BS solution and its main constituents, namely MB and AMX. That is, the interaction between BS and the adsorbent caused changes in the general functional groups. On the onther hand, C−O functional group was located at ∼1060 cm^{-1} (185).

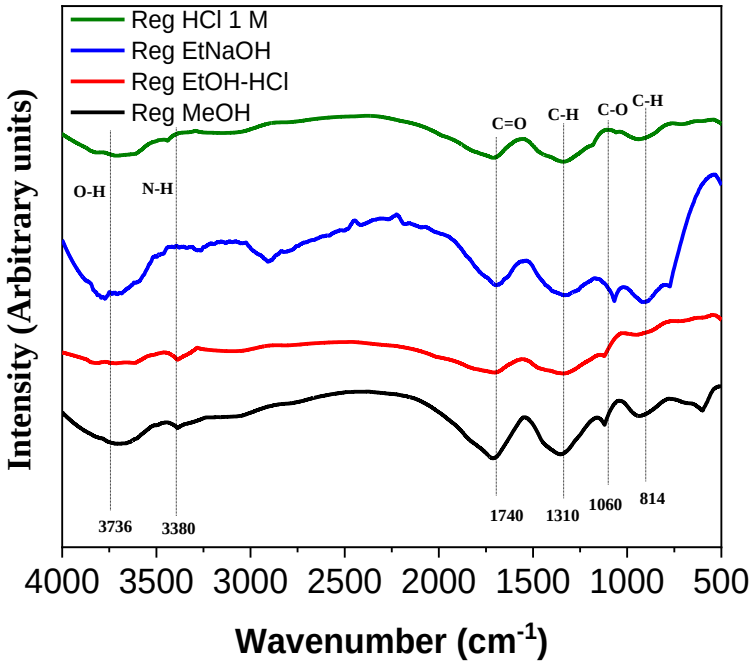

Figure 5.18: FTIR analysis for regenerated activated carbon samples.

5.11 General comparison for macadamia nutshell activated carbons

Table 5.11 provides knowledge about previous recent works where macadamia nutshell was used as a precursor. Data presented in the table contains information regarding the maximum adsorption capacity reached through using their methods for primarily one pollutant, which in all cases are lesser than the results shown in the presented work.

Table 5.11: Comparative chart of the removal achieved by activated carbons produced from macadamia nutshell.

Ref.	Pollutant	Activation method	Maximum adsorption capacity [mg/g]
(186)	Melanoidin	-	14.7
(187)	Methylene Blue	Physical activation	97
(34)	Methylene Blue	Physical activation	134.69
(188)	Reactive Blue 19	Chemical activation (KOH)	376.81
(189)	Methylene Blue	-	444.732
(146)	Methylene Blue	Physical activation	41.83
(32)	Tetracycline	Chemical activation (NaOH)	455.33
This work	Methylene blue and amoxicillin	Chemical activation (K_2CO_3)	788.305

Likewise, (as mentioned in the previous sections) some of the additional qualities of the activated carbon produced in this thesis project reside in the materials used for its preparation. These materials are environment-friendly. On the one hand, macadamia nut shell is considered a lignocellulosic residue; besides, the use of K_2CO_3 as an activating agent reduces harmful effects on the environment. Also, it can work in neutral pH environments and shows good results when simultaneously adsorbing two contaminants.

Chapter 6

Conclusions and recommendations

In conclusions, microporous activated carbon was developed from macadamia nutshell (MNS) using potassium carbonate as eco-friendly activation agent. The Box-Behnken toolbox allowed for generation of experimental design (15 experimental runs) to evaluate the influence of factors such as K_2CO_3: precursor ratio, activation temperature, and activation time on the response surface for binary adsorption of cationic methylene blue dye and ionic amoxicillin antibiotics.

Under optimal conditions of 900 °C, 1 h and K_2CO_3: precursor ratio of 2:1, the Run 2 sample revealed a specific surface area of 1225 m^2/g, pore volume of 0.801 cm^3/g, and an average pore width of 0.406 nm.

It was found that the pyrolysis temperature was the factor that most influenced the properties of the resulting activated carbons (p-value=0.004<0.05= α) , which were directly reflected in the yield and percentage of BS removal. Likewise, the interaction of factors that most affected the response variables was temperature-time. The central points of the experimental design demonstrate good data collection and experimental reproducibility.

The Run 2 activated carbon realized a maximum adsorption capacity of 788.305 mg/g under best conditions of 40 °C and neutral pH. The pseudo second order adsorption kinetic model adequately described the experimental data with RMSE, ARE and R^2 in the range of 0.552-87.57, 0.008-0.082, 0.999-0.947, respectively, which indicates chemisorption mechanism. Evaluated isotherm models revealed that Khan isotherm used for pure substances best described the variation in the data. Thermodynamic studies show an exothermic adsorption at low concentration experiments and endothermic for the ones at high concentrations.

The regeneration process with the best performance was carried out using a mixture of ethanol and sodium hydroxide. However, the characterization studies showed a loss in the textural properties of the activated carbon samples subjected to this regeneration process. After 5 cycles of regeneration processes, the activated carbon sample remained with a DFT surface area of 27.976 m^2/g and a pore volume of 0.072 m^3/g.

As a future work, it is proposed to focus efforts on the search for activated carbon production methodologies that are energetically more environmentally friendly. Likewise, the implementation of equipment that has the ability to monitor in real-time the adsorption in order to obtain more accurate results and improve their analysis. Additionally, it is appropriate to continue searching for new lignocellulosic materials that allow for the obtaining of activated carbons with good adsorbent properties.

Appendix A

Additional information

A.1 Calibration curves

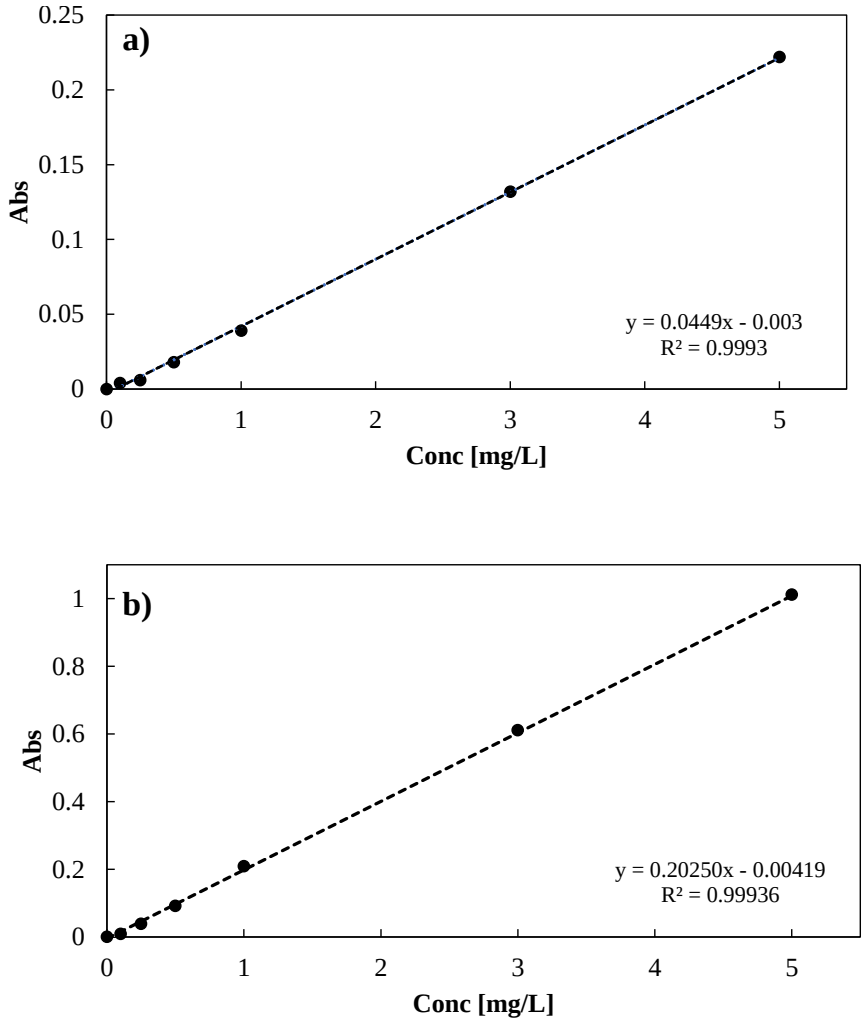

Figure A.1: Calibration curves to determinate the concentration of a) AMX and b) MB contained on BS.

A.2 Constants of the intraparticle diffusion study of Weber and Morris.

Table A.1: Interparticle diffusion analysis.

Temp.(°)	30						40						50					
BS conc. (mg/L)	50	100	200	400	600	800	50	100	200	400	600	800	50	100	200	400	600	800
Slope 1																		
ki_1	26.64	53.14	124.03	176.80	147.91	153.88	26.46	54.83	105.87	194.68	235.64	214.23	26.14	49.69	125.83	164.59	168.27	188.49
C_1	4.62	9.25	23.75	34.66	28.57	21.16	4.44	9.65	20.05	29.08	32.82	24.05	4.71	11.10	23.15	25.60	24.08	33.02
R^2	0.96	0.97	0.96	0.96	0.96	0.98	0.97	0.97	0.96	0.98	0.98	0.99	0.97	0.95	0.97	0.97	0.98	0.97
Slope 2																		
ki_2	0.03	1.19	0.63	8.01	10.86	11.52	0.03	0.02	2.51	2.25	5.75	7.68	0.01	2.02	0.50	4.84	7.55	10.06
C_2	53.29	109.68	267.36	360.98	310.71	319.68	55.53	118.57	225.60	443.88	558.94	500.00	55.05	105.69	298.68	405.68	410.98	459.45
R^2	0.88	0.81	0.97	0.99	0.98	1.00	0.96	0.93	0.94	0.91	0.97	0.99	0.96	0.97	0.97	0.98	0.98	0.99
Slope 3																		
ki_3				0.18	11.95	10.68			0.49					0.01				
C_3				542.42	110.42	239.46			241.11					118.31				
R^2				0.998	0.97	0.93			0.99					0.98				

With C_i as the intercept value in (mg/g), and the rate constant k_i in (mg /g $min^{1/2}$).

A.3 Experimental kinetic data obtained at different BS concentrations and temperature

Table A.2: Parameters and errors obtained from the adsorption kinetics models were adjusted to the experimental data carried out at 30 °C.

Exp	q_e	Pseudo first-order					Pseudo second-order					Elovich					
		q_{cal}	k_1	R^2	RMSE	ARE	q_{cal}	k_2	R^2	RMSE	ARE	q_{cal}	β	α	R^2	RMSE	ARE
E@50	54.311	54.311	1.582	0.999	0.840	0.011	53.763	0.192	0.999	0.537	0.008	54.555	0.405	1.22E+06	0.999	0.371	0.005
E@100	118.984	118.984	1.267	0.998	2.339	0.012	117.647	0.045	0.999	1.255	0.009	120.135	0.496	1.17E+20	0.999	1.218	0.009
E@200	292.907	292.907	1.154	0.993	16.608	0.049	277.778	0.019	0.996	7.894	0.023	290.779	0.060	7.73E+04	0.999	2.538	0.006
E@400	549.936	549.936	0.584	0.942	83.722	0.151	476.190	0.003	0.947	49.983	0.096	545.200	0.028	5.98E+03	0.992	13.999	0.024
E@600	596.971	596.971	0.376	0.941	106.808	0.201	526.316	0.000	0.944	69.543	0.124	570.018	0.024	9.02E+02	0.990	18.194	0.032
E@800	658.010	658.010	0.299	0.913	140.579	0.249	526.316	0.000	0.927	81.796	0.138	628.160	0.021	4.43E+02	0.985	25.551	0.051

Table A.3: Parameters and errors obtained from the adsorption kinetics models were adjusted to the experimental data carried out at 40 °C.

Exp	q_e	Pseudo first-order					Pseudo second-order					Elovich					
		q_{cal}	k_1	R^2	RMSE	ARE	q_{cal}	k_2	R^2	RMSE	ARE	q_{cal}	β	α	R^2	RMSE	ARE
E@50	56.416	56.416	0.934	0.992	1.517	0.015	55.866	0.291	0.999	0.552	0.008	55.991	9.911	6.41E+236	0.998	0.632	0.009
E@100	119.618	119.618	0.639	0.974	5.739	0.016	119.048	0.078	1.000	0.595	0.004	120.110	1.660	1.46E+83	0.999	0.961	0.007
E@200	260.475	260.475	0.352	0.923	23.250	0.061	250.000	0.013	0.995	7.200	0.025	260.349	0.180	8.27E+17	0.999	2.014	0.005
E@400	527.043	527.043	0.291	0.916	57.064	0.097	476.190	0.003	0.984	28.578	0.047	527.046	0.050	3.70E+09	0.994	11.078	0.013
E@600	788.305	788.305	0.051	0.835	128.274	0.223	714.286	0.000	0.959	62.771	0.124	769.533	0.017	1.50E+04	0.994	13.171	0.016
E@800	769.991	769.991	0.092	0.844	150.069	0.168	666.667	0.001	0.947	85.571	0.082	765.532	0.021	3.04E+05	0.997	18.924	0.028

Table A.4: Parameters and errors obtained from the adsorption kinetics models were adjusted to the experimental data carried out at 50 °C.

Exp	q_e	Pseudo first-order					Pseudo second-order					Elovich					
		q_{cal}	k_1	R^2	RMSE	ARE	q_{cal}	k_2	R^2	RMSE	ARE	q_{cal}	β	α	R^2	RMSE	ARE
E@50	55.713	55.713	1.918	0.998	1.146	0.017	46.296	1.104	0.999	0.591	0.009	54.335	0.405	1.22E+06	0.999	0.538	0.008
E@100	119.853	119.853	1.337	0.989	4.367	0.023	103.093	0.011	0.979	5.197	0.015	120.368	0.496	1.17E+20	0.994	2.621	0.017
E@200	291.387	291.387	1.184	0.992	12.845	0.037	232.558	0.022	0.995	6.897	0.018	290.073	0.060	7.73E+04	0.9998	1.283	0.004
E@400	534.862	534.862	0.198	0.820	101.229	0.208	357.143	0.003	0.879	54.312	0.099	520.296	0.028	5.98E+03	0.988	16.763	0.034
E@600	628.621	628.621	0.039	0.816	128.786	0.246	333.333	0.001	0.852	73.817	0.129	604.133	0.024	9.02E+02	0.987	22.293	0.041
E@800	758.391	758.391	0.021	0.803	166.373	0.273	357.143	0.000	0.825	99.894	0.154	719.060	0.021	4.43E+02	0.970	40.953	0.063

A.4 Complete parameters of the isotherms

Table A.5: Data obtained from several isotherm models at different temperatures.

	303 K	313 K	323 K
Langmuir			
q_m	625.000	833.333	714.286
K_L	0.364	0.130	0.226
R_L	0.047-0.0028	0.0453-0.0026	0.0464-0.0025
R^2	0.971	0.949	0.945
Freundlich			
n_F	2.947	2.422	2.848
K_F	112.694	96.272	112.902
R^2	0.893	0.921	0.919
Temkin			
B_i	93.955	132.160	85.112
K_T	4.166	1.701	45.496
R^2	0.964	0.980	0.964
Sips			
K_s	0.221	0.117	0.195
n_s	0.608	1.601	1.755
q_m	603.201	1016.144	848.560
R^2	0.970	0.973	0.957
Dubinin-Radushkevich			
B	5.00E-07	8.00E-07	2.00E-06
q_m	568.272	568.272	453.820
R^2	0.924	0.889	0.917
Liu			
q_m	505.3744	1016.388	848.9805
k_L	0.00158	0.03209	0.05668
n_L	13.73751	0.62426	0.56939
R^2	0.27985	0.966	0.961
Redlich-Peterson			
K_{RP}	192.3549	136.2447	220.5415
a_{RP}	0.41113	0.38443	0.63704
n_{RP}	0.94393	0.84852	0.87145
R^2	0.977	0.967	0.973
Khan			
q_m	467.926	386.2639	349.2194
K_K	0.39745	0.31641	0.5623
n_K	0.93297	0.833114	0.85935
R^2	0.978	0.967	0.975

Bibliography

[1] S. Wong, N. Ngadi, I. M. Inuwa, and O. Hassan, "Recent advances in applications of activated carbon from biowaste for wastewater treatment: a short review," *Journal of Cleaner Production*, vol. 175, pp. 361–375, 2018. 1

[2] R. Anjali and S. Shanthakumar, "Insights on the current status of occurrence and removal of antibiotics in wastewater by advanced oxidation processes," *Journal of environmental management*, vol. 246, pp. 51–62, 2019. 1

[3] W. H. Organization *et al.*, "Guidelines for drinking-water quality: incorporating the first and second addenda," tech. rep., WHO: World Health Organization, 2022. 1

[4] World Health Organization, "World health statistics 2022 (Monitoring health of the SDGs)," tech. rep., WHO, 2022. 1

[5] T. Deblonde, C. Cossu-Leguille, and P. Hartemann, "Emerging pollutants in wastewater: a review of the literature," *International journal of hygiene and environmental health*, vol. 214, no. 6, pp. 442–448, 2011. 1

[6] D. R. Lobato-Peralta, E. Duque-Brito, A. Ayala-Cortés, A. D. María, A. Longoria, A. K. Cuentas-Gallegos, P. Sebastian, and P. U. Okoye, "Advances in activated carbon modification, surface heteroatom configuration, reactor strategies, and regeneration methods for enhanced wastewater treatment," *Journal of Environmental Chemical Engineering*, p. 105626, 2021. 1, 2, 5, 22

[7] F. C. Moura, R. D. Rios, and B. R. Galvão, "Emerging contaminants removal by granular activated carbon obtained from residual macauba biomass," *Environmental Science and Pollution Research*, vol. 25, no. 26, pp. 26482–26492, 2018. 1

[8] M. C. Collivignarelli, A. Abbà, I. Benigna, S. Sorlini, and V. Torretta, "Overview of the main disinfection processes for wastewater and drinking water treatment plants," *Sustainability*, vol. 10, no. 1, p. 86, 2018. 1

[9] G. Crini and E. Lichtfouse, "Advantages and disadvantages of techniques used for wastewater treatment," *Environmental Chemistry Letters*, vol. 17, no. 1, pp. 145–155, 2019. 1, 2

[10] R. C. Bansal and M. Goyal, *Activated carbon adsorption*. CRC press, 2005. 2

[11] V. H. Montoya and A. Bonilla-Petriciolet, *Lignocellulosic precursors used in the synthesis of activated carbon: characterization techniques and applications in the wastewater treatment*. BoD–Books on Demand, 2012. 2

[12] Z. Jeirani, C. H. Niu, and J. Soltan, "Adsorption of emerging pollutants on activated carbon," *Reviews in Chemical Engineering*, vol. 33, no. 5, pp. 491–522, 2017. 2, 41

[13] F. Marrakchi, M. Auta, W. Khanday, and B. Hameed, "High-surface-area and nitrogen-rich mesoporous carbon material from fishery waste for effective adsorption of methylene blue," *Powder Technology*, vol. 321, pp. 428–434, 2017. 2

[14] P. Li, W. Feng, C. Xue, R. Tian, and S. Wang, "Spatiotemporal variability of contaminants in lake water and their risks to human health: a case study of the shahu lake tourist area, northwest china," *Exposure and health*, vol. 9, pp. 213–225, 2017. 2

[15] B. Acevedo and C. Barriocanal, "Texture and surface chemistry of activated carbons obtained from tyre wastes," *Fuel Processing Technology*, vol. 134, pp. 275–283, 2015. 5

[16] P. González-García, "Activated carbon from lignocellulosics precursors: A review of the synthesis methods, characterization techniques and applications," *Renewable and Sustainable Energy Reviews*, vol. 82, pp. 1393–1414, 2018. 5

[17] D. Duan, D. Chen, L. Huang, Y. Zhang, Y. Zhang, Q. Wang, G. Xiao, W. Zhang, H. Lei, and R. Ruan, "Activated carbon from lignocellulosic biomass as catalyst: A review of the applications in fast pyrolysis process," *Journal of Analytical and Applied Pyrolysis*, vol. 158, p. 105246, 2021. 5, 13

[18] Transparency Market Research, "Activated Carbon Market Size, Growth, Trands, Analysis - 2031," tech. rep., Transparency Market Research, 2022. 5

[19] F. Çeçen and Ö. Aktaş, *Fundamentals of Adsorption onto Activated Carbon in Water and Wastewater Treatment*, ch. 2, pp. 13–41. John Wiley & Sons, Ltd, 2011. 5

[20] M. Bastidas, L. M. Buelvas, M. I. Márquez, and K. Rodríguez, "Producción de carbón activado a partir de precursores carbonosos del departamento del cesar, colombia," *Información tecnológica*, vol. 21, no. 3, pp. 87–96, 2010. 5

[21] E. K. Putra, R. Pranowo, J. Sunarso, N. Indraswati, and S. Ismadji, "Performance of activated carbon and bentonite for adsorption of amoxicillin from wastewater: mechanisms, isotherms and kinetics," *Water research*, vol. 43, no. 9, pp. 2419–2430, 2009. 5

[22] World Health Organization, "Who report on surveillance of antibiotic consumption," tech. rep., WHO: World Health Organization, 2018. 6

[23] M. A. E. de Franco, C. B. de Carvalho, M. M. Bonetto, R. de Pelegrini Soares, and L. A. Féris, "Removal of amoxicillin from water by adsorption onto activated carbon in batch process and fixed bed column: kinetics, isotherms, experimental design and breakthrough curves modelling," *Journal of Cleaner Production*, vol. 161, pp. 947–956, 2017. 6

[24] O. Pezoti, A. L. Cazetta, K. C. Bedin, L. S. Souza, A. C. Martins, T. L. Silva, O. O. S. Júnior, J. V. Visentainer, and V. C. Almeida, "Naoh-activated carbon of high surface area produced from guava seeds as a high-efficiency adsorbent for amoxicillin removal: Kinetic, isotherm and thermodynamic studies," *Chemical Engineering Journal*, vol. 288, pp. 778–788, 2016. 6

[25] C. Suárez and F. Gudiol, "Antibióticos betalactámicos," *Enfermedades infecciosas y microbiología clínica*, vol. 27, no. 2, pp. 116–129, 2009. 6

[26] S. A. Gupta, Y. Vishesh, N. Sarvshrestha, A. S. Bhardwaj, P. A. Kumar, N. S. Topare, S. Raut-Jadhav, S. A. Bokil, and A. Khan, "Adsorption isotherm studies of methylene blue using activated carbon of waste fruit peel as an adsorbent," *Materials Today: Proceedings*, 2021. 6

[27] S. A. Borghei, M. H. Zare, M. Ahmadi, M. H. Sadeghi, A. Marjani, S. Shirazian, and M. Ghadiri, "Synthesis of multi-application activated carbon from oak seeds by koh activation for methylene blue adsorption and electrochemical supercapacitor electrode," *Arabian Journal of Chemistry*, vol. 14, no. 2, p. 102958, 2021. 6

[28] M. A. Al-Ghouti and A. O. Sweleh, "Optimizing textile dye removal by activated carbon prepared from olive stones," *Environmental Technology & Innovation*, vol. 16, p. 100488, 2019. 6

[29] Y. Zhu, P. Kolar, S. B. Shah, J. J. Cheng, and P. Lim, "Simultaneous mitigation of p-cresol and ammonium using activated carbon from avocado seed," *Environmental Technology & Innovation*, vol. 9, pp. 63–73, 2018. 6

[30] L. S. Chan, W. Cheung, S. J. Allen, and G. McKay, "Equilibrium adsorption isotherm study of binary basic dyes on to bamboo derived activated carbon," *HKIE transactions*, vol. 24, no. 4, pp. 182–192, 2017. 6

[31] S. Benhabiles and K. Rida, "Production of efficient activated carbon from sawdust for the removal of dyes in single and binary systems–a full factorial design," *Particulate Science and Technology*, vol. 39, no. 2, pp. 237–251, 2021. 6, 21

[32] A. C. Martins, O. Pezoti, A. L. Cazetta, K. C. Bedin, D. A. Yamazaki, G. F. Bandoch, T. Asefa, J. V. Visentainer, and V. C. Almeida, "Removal of tetracycline by naoh-activated carbon produced from macadamia nut shells: kinetic and equilibrium studies," *Chemical Engineering Journal*, vol. 260, pp. 291–299, 2015. 7, 47, 60

[33] S. Wongcharee, V. Aravinthan, and L. Erdei, "Mesoporous activated carbon-zeolite composite prepared from waste macadamia nut shell and synthetic faujasite," *Chinese journal of chemical engineering*, vol. 27, no. 1, pp. 226–236, 2019. 7, 38

[34] S. Wongcharee, V. Aravinthan, L. Erdei, and W. Sanongraj, "Mesoporous activated carbon prepared from macadamia nut shell waste by carbon dioxide activation: C omparative characterisation and study of methylene blue removal from aqueous solution," *Asia-Pacific Journal of Chemical Engineering*, vol. 13, no. 2, p. e2179, 2018. 7, 55, 60

[35] T. M. Dao and T. Le Luu, "Synthesis of activated carbon from macadamia nutshells activated by h2so4 and k2co3 for methylene blue removal in water," *Bioresource Technology Reports*, vol. 12, p. 100583, 2020. 7

[36] K. Karimi, *Lignocellulose-based bioproducts*. Springer, 2015. 9

[37] G. Velvizhi, C. Goswami, N. P. Shetti, E. Ahmad, K. K. Pant, and T. M. Aminabhavi, "Valorisation of lignocellulosic biomass to value-added products: Paving the pathway towards low-carbon footprint," *Fuel*, vol. 313, p. 122678, 2022. 9

[38] A. Akbarian, A. Andooz, E. Kowsari, S. Ramakrishna, S. Asgari, and Z. A. Cheshmeh, "Challenges and opportunities of lignocellulosic biomass gasification in the path of circular bioeconomy," *Bioresource Technology*, p. 127774, 2022. 9

[39] H. Treichel, G. Fongaro, T. Scapini, A. Frumi Camargo, F. Spitza Stefanski, and B. Venturin, *Structure of Residual Biomass Characterization*, pp. 7–18. Cham: Springer International Publishing, 2020. 9

[40] S. Wang, G. Dai, H. Yang, and Z. Luo, "Lignocellulosic biomass pyrolysis mechanism: A state-of-the-art review," *Progress in energy and combustion science*, vol. 62, pp. 33–86, 2017. 9, 12, 13

[41] J. Cheng, *Biomass to renewable energy processes*. CRC press, 2017. 9, 11

[42] W. O. Doherty, P. Mousavioun, and C. M. Fellows, "Value-adding to cellulosic ethanol: Lignin polymers," *Industrial crops and products*, vol. 33, no. 2, pp. 259–276, 2011. 9

[43] V. K. Yadav, N. Gupta, P. Kumar, M. G. Dashti, V. Tirth, S. H. Khan, K. K. Yadav, S. Islam, N. Choudhary, A. Algahtani, *et al.*, "Recent advances in synthesis and degradation of lignin and lignin nanoparticles and their emerging applications in nanotechnology," *Materials*, vol. 15, no. 3, p. 953, 2022. 9

[44] A. J. Sayyed, D. V. Pinjari, S. H. Sonawane, B. A. Bhanvase, J. Sheikh, and M. Sillanpää, "Cellulose-based nanomaterials for water and wastewater treatments: A review," *Journal of Environmental Chemical Engineering*, vol. 9, no. 6, p. 106626, 2021. 10

[45] K. Liu, H. Du, T. Zheng, H. Liu, M. Zhang, R. Zhang, H. Li, H. Xie, X. Zhang, M. Ma, *et al.*, "Recent advances in cellulose and its derivatives for oilfield applications," *Carbohydrate Polymers*, vol. 259, p. 117740, 2021. 10

[46] E. Duque-Brito, *Comparación de técnicas de caracterización de biomasas lignocelulósicas*. PhD thesis, Universidad Nacional Autónoma de México, 2021. 10, 35

[47] Z. Azwa, B. Yousif, A. Manalo, and W. Karunasena, "A review on the degradability of polymeric composites based on natural fibres," *Materials & Design*, vol. 47, pp. 424–442, 2013. 10

[48] K. Liu, H. Du, T. Zheng, W. Liu, M. Zhang, H. Liu, X. Zhang, and C. Si, "Lignin-containing cellulose nanomaterials: preparation and applications," *Green Chemistry*, vol. 23, no. 24, pp. 9723–9746, 2021. 10

[49] H. Treichel, G. Fongaro, T. Scapini, A. Frumi Camargo, F. Spitza Stefanski, and B. Venturin, *Utilising biomass in biotechnology*. Springer, 2020. 10

[50] M. F. Qaseem, H. Shaheen, and A.-M. Wu, "Cell wall hemicellulose for sustainable industrial utilization," *Renewable and Sustainable Energy Reviews*, vol. 144, p. 110996, 2021. 11

[51] L.-Z. Huang, M.-G. Ma, X.-X. Ji, S.-E. Choi, and C. Si, "Recent developments and applications of hemicellulose from wheat straw: A review," *Frontiers in Bioengineering and Biotechnology*, vol. 9, p. 690773, 2021. 11

[52] W. Hu, M. Fitzgerald, B. Topp, M. Alam, and T. J. O'Hare, "A review of biological functions, health benefits, and possible de novo biosynthetic pathway of palmitoleic acid in macadamia nuts," *Journal of Functional Foods*, vol. 62, p. 103520, 2019. 11

[53] L. Mapel-Velazco, "Caracterización física y química de la nuez y el aceite de variedades e híbridos de macadamia integrifolia y macadamia tetraphylla cultivadas en coatepec, veracruz.," Master's thesis, Uiversidad Veracruzana: Instituto de Ciencias Básicas, 2014. 11, 12

[54] T. Kaseke, O. A. Fawole, and U. L. Opara, "Chemistry and functionality of cold-pressed macadamia nut oil," *Processes*, vol. 10, no. 1, p. 56, 2021. 11

[55] SAGARPA, "Macadamia, la nuez más fina del mundo," *Claridades Agropecuarias*, vol. 81, pp. 3–citation_lastpage, 2000. 11

[56] International Nut & Dried Fruit Council, "Nuts & Dried Fruits - Statistical Yearbook 2019-2020," tech. rep., International Nut & Dried Fruit Council, 2020. 11

[57] SAMAC, "Industry Statistics," 2021. 11

[58] SIAP, "Datos Abiertos," tech. rep., Servicio de Información Agroalimentaria y Pesquera, 2021. 11

[59] A. Wechsler, M. Zaharia, A. Crosky, H. Jones, M. Ramírez, A. Ballerini, M. Nuñez, and V. Sahajwalla, "Macadamia (macadamia integrifolia) shell and castor (rícinos communis) oil based sustainable particleboard: A comparison of its properties with conventional wood based particleboard," *Materials & Design*, vol. 50, pp. 117–123, 2013. 12

[60] X. Carrera and R. Carrera, "Plan de negocios para la comercialización y exportación de la nuez de macadamia hacia el mercado norteamericano," B.S. thesis, UIDE, 2011. 12

[61] K. Januszewicz, P. Kazimierski, M. Klein, D. Kardaś, and J. Łuczak, "Activated carbon produced by pyrolysis of waste wood and straw for potential wastewater adsorption," *Materials*, vol. 13, no. 9, p. 2047, 2020. 12

[62] S. Ascher, I. Watson, and S. You, "Machine learning methods for modelling the gasification and pyrolysis of biomass and waste," *Renewable and Sustainable Energy Reviews*, vol. 155, p. 111902, 2022. 12

[63] S. Y. Foong, Y. H. Chan, W. Y. Cheah, N. H. Kamaludin, T. N. B. T. Ibrahim, C. Sonne, W. Peng, P.-L. Show, and S. S. Lam, "Progress in waste valorization using advanced pyrolysis techniques for hydrogen and gaseous fuel production," *Bioresource technology*, vol. 320, p. 124299, 2021. 12

[64] F. Cheng, H. Luo, and L. M. Colosi, "Slow pyrolysis as a platform for negative emissions technology: An integration of machine learning models, life cycle assessment, and economic analysis," *Energy Conversion and Management*, vol. 223, p. 113258, 2020. 13

[65] M. Uddin, K. Techato, J. Taweekun, M. M. Rahman, M. Rasul, T. Mahlia, and S. Ashrafur, "An overview of recent developments in biomass pyrolysis technologies," *Energies*, vol. 11, no. 11, p. 3115, 2018. 13

[66] H. C. Ong, K. L. Yu, W.-H. Chen, M. K. Pillejera, X. Bi, K.-Q. Tran, A. Pétrissans, and M. Pétrissans, "Variation of lignocellulosic biomass structure from torrefaction: A critical review," *Renewable and Sustainable Energy Reviews*, vol. 152, p. 111698, 2021. 13

[67] F. Ronsse, R. W. Nachenius, and W. Prins, "Carbonization of biomass," in *Recent advances in thermo-chemical conversion of biomass*, pp. 293–324, Elsevier, 2015. 13

[68] M. Harussani, S. Sapuan, A. Khalina, R. Ilyas, and M. Hazrol, "Review on green technology pyrolysis for plastic wastes," in *Proceedings of the 7th Postgraduate Seminar on Natural Fibre Reinforced Polymer Composites*, pp. 50–53, 2020. 13

[69] J. D. Martínez, N. Puy, R. Murillo, T. García, M. V. Navarro, and A. M. Mastral, "Waste tyre pyrolysis–a review," *Renewable and sustainable energy reviews*, vol. 23, pp. 179–213, 2013. 13

[70] T. Kan, V. Strezov, and T. J. Evans, "Lignocellulosic biomass pyrolysis: A review of product properties and effects of pyrolysis parameters," *Renewable and sustainable energy reviews*, vol. 57, pp. 1126–1140, 2016. 13

[71] M. Gayathiri, T. Pulingam, K. Lee, and K. Sudesh, "Activated carbon from biomass waste precursors: Factors affecting production and adsorption mechanism," *Chemosphere*, p. 133764, 2022. 13, 14, 20

[72] J. Muñiz, N. D. Espinosa-Torres, A. Guillén-López, A. Longoria, A. K. Cuentas-Gallegos, and M. Robles, "Insights into the design of carbon electrodes coming from lignocellulosic components pyrolysis with potential application in energy storage devices: a combined in silico and experimental study," *Journal of Analytical and Applied Pyrolysis*, vol. 139, pp. 131–144, 2019. 13

[73] S. Wang, B. Ru, G. Dai, W. Sun, K. Qiu, and J. Zhou, "Pyrolysis mechanism study of minimally damaged hemicellulose polymers isolated from agricultural waste straw samples," *Bioresource technology*, vol. 190, pp. 211–218, 2015. 13

[74] T. Hosoya, H. Sato, and S. Sakaki, "Thermal decomposition of cellulose: Difference between single chain and multiple chains," in *the 4th Molecular Science Conference*, p. 1P107, 2010. 13

[75] M. Tripathi, J. N. Sahu, and P. Ganesan, "Effect of process parameters on production of biochar from biomass waste through pyrolysis: A review," *Renewable and sustainable energy reviews*, vol. 55, pp. 467–481, 2016. 13

[76] K. S. Ukanwa, K. Patchigolla, R. Sakrabani, E. Anthony, and S. Mandavgane, "A review of chemicals to produce activated carbon from agricultural waste biomass," *Sustainability*, vol. 11, no. 22, p. 6204, 2019. 13

[77] J. Ouyang, L. Zhou, Z. Liu, J. Y. Heng, and W. Chen, "Biomass-derived activated carbons for the removal of pharmaceutical mircopollutants from wastewater: A review," *Separation and Purification Technology*, vol. 253, p. 117536, 2020. 14

[78] M. S. Reza, C. S. Yun, S. Afroze, N. Radenahmad, M. S. A. Bakar, R. Saidur, J. Taweekun, and A. K. Azad, "Preparation of activated carbon from biomass and its' applications in water and gas purification, a review," *Arab Journal of Basic and Applied Sciences*, vol. 27, no. 1, pp. 208–238, 2020. 14

[79] P. Sinha, S. Banerjee, and K. K. Kar, "Characteristics of activated carbon," *Handbook of Nanocomposite Supercapacitor Materials I: Characteristics*, pp. 125–154, 2020. 14

[80] A. Bonilla-Petriciolet, D. I. Mendoza-Castillo, and H. E. Reynel-Ávila, *Adsorption processes for water treatment and purification*, vol. 256. Springer, 2017. 14, 16, 51

[81] M. Alaqarbeh, "Adsorption phenomena: Definition, mechanisms, and adsorption types: Short review," *RHAZES: Green and Applied Chemistry*, vol. 13, pp. 43–51, 2021. 14

[82] C. P. Bergmann and F. M. Machado, *Carbon nanomaterials as adsorbents for environmental and biological applications*. Springer, 2015. 14, 21, 44

[83] H. Qiu, L. Lv, B.-c. Pan, Q.-j. Zhang, W.-m. Zhang, and Q.-x. Zhang, "Critical review in adsorption kinetic models," *Journal of Zhejiang University-Science A*, vol. 10, no. 5, pp. 716–724, 2009. 15, 16

[84] V. Bolis, "Fundamentals in adsorption at the solid-gas interface. concepts and thermodynamics," *Calorimetry and thermal methods in catalysis*, pp. 3–50, 2013. 15

[85] J. Wang and X. Guo, "Adsorption kinetic models: Physical meanings, applications, and solving methods," *Journal of Hazardous materials*, vol. 390, p. 122156, 2020. 15, 17, 50

[86] T. R. Sahoo and B. Prelot, "Adsorption processes for the removal of contaminants from wastewater: the perspective role of nanomaterials and nanotechnology," in *Nanomaterials for the detection and removal of wastewater pollutants*, pp. 161–222, Elsevier, 2020. 15, 16, 17, 50

[87] S. Lagergren, "About the theory of so-called adsorption of soluble substances," *Vetenskapsakademies Handl.*, pp. 1–39, 1898. 16, 30

[88] L. Largitte and R. Pasquier, "A review of the kinetics adsorption models and their application to the adsorption of lead by an activated carbon," *Chemical engineering research and design*, vol. 109, pp. 495–504, 2016. 16

[89] S. S. Ray, R. Gusain, and N. Kumar, "Adsorption equilibrium isotherms, kinetics and thermodynamics," in *Carbon Nanomaterial-Based Adsorbents for Water Purification*, pp. 101–118, Elsevier, 2020. 16, 54

[90] E. D. Revellame, D. L. Fortela, W. Sharp, R. Hernandez, and M. E. Zappi, "Adsorption kinetic modeling using pseudo-first order and pseudo-second order rate laws: A review," *Cleaner Engineering and Technology*, vol. 1, p. 100032, 2020. 16, 50

[91] M. E. González-López, C. M. Laureano-Anzaldo, A. A. Pérez-Fonseca, M. Arellano, and J. R. Robledo-Ortíz, "A critical overview of adsorption models linearization: methodological and statistical inconsistencies," *Separation & Purification Reviews*, vol. 51, no. 3, pp. 358–372, 2022. 16, 18

[92] Y. S. Ho and G. McKay, "Pseudo-second order model for sorption processes," *Process Biochemistry*, vol. 34, pp. 451–465, jul 1999. 16, 30, 51

[93] S. Elovich and O. Larinov, "Theory of adsorption from solutions of non-electrolytes on solid (I) equation adsorption from solutions and the analysis of its simplest form, (II) verification of the equation of adsorption isotherm from solutions," *Izv. Akad. Nauk. SSSR, Otd. Khim. Nauk.*, vol. 2, pp. 209–216, 1962. 16, 30

[94] S. Edebali, *Advanced sorption process applications*. IntechOpen, 2019. 16

[95] L. M. Silva, M. J. Muñoz-Peña, J. R. Domínguez-Vargas, T. González, and E. M. Cuerda-Correa, "Kinetic and equilibrium adsorption parameters estimation based on a heterogeneous intraparticle diffusion model," *Surfaces and Interfaces*, vol. 22, p. 100791, 2021. 17

[96] M. Schwaab, E. Steffani, E. Barbosa-Coutinho, and J. B. S. Júnior, "Critical analysis of adsorption/diffusion modelling as a function of time square root," *Chemical Engineering Science*, vol. 173, pp. 179–186, 2017. 17

[97] K. Y. Foo and B. H. Hameed, "Insights into the modeling of adsorption isotherm systems," *Chemical engineering journal*, vol. 156, no. 1, pp. 2–10, 2010. 17, 18, 52

[98] M. A. Al-Ghouti and D. A. Da'ana, "Guidelines for the use and interpretation of adsorption isotherm models: A review," *Journal of hazardous materials*, vol. 393, p. 122383, 2020. 17, 18, 53

[99] I. Langmuir, "The constitution and fundamental properties of solids and liquids. part i. solids.," *Journal of the American chemical society*, vol. 38, no. 11, pp. 2221–2295, 1916. 18, 31

[100] S. Kalam, S. A. Abu-Khamsin, M. S. Kamal, and S. Patil, "Surfactant adsorption isotherms: A review," *ACS omega*, vol. 6, no. 48, pp. 32342–32348, 2021. 18, 53

[101] X. Guo and J. Wang, "Comparison of linearization methods for modeling the langmuir adsorption isotherm," *Journal of Molecular Liquids*, vol. 296, p. 111850, 2019. 18

[102] M. M. Majd, V. Kordzadeh-Kermani, V. Ghalandari, A. Askari, and M. Sillanpää, "Adsorption isotherm models: A comprehensive and systematic review (2010-2020)," *Science of The Total Environment*, vol. 812, p. 151334, 2022. 18, 19, 52

[103] M. Rajabi, S. Keihankhadiv, I. Tyagi, R. R. Karri, M. Chaudhary, N. M. Mubarak, S. Chaudhary, P. Kumar, and P. Singh, "Comparison and interpretation of isotherm models for the adsorption of dyes, proteins, antibiotics, pesticides and heavy metal ions on different nanomaterials and non-nano materials—a

comprehensive review," *Journal of Nanostructure in Chemistry*, vol. 13, no. 1, pp. 43–65, 2023. 18

[104] H. Freundlich, "Over the adsorption in solution," *Journal of Physical Chemistry*, vol. 57, p. e470, 1906. 18, 31

[105] X. Chen, M. F. Hossain, C. Duan, J. Lu, Y. F. Tsang, M. S. Islam, and Y. Zhou, "Isotherm models for adsorption of heavy metals from water-a review," *Chemosphere*, p. 135545, 2022. 18

[106] A. R. Khan, I. Al-Waheab, and A. Al-Haddad, "A generalized equation for adsorption isotherms for multi-component organic pollutants in dilute aqueous solution," *Environmental technology*, vol. 17, no. 1, pp. 13–23, 1996. 18, 31

[107] A. Syafiuddin, S. Salmiati, J. Jonbi, and M. A. Fulazzaky, "Application of the kinetic and isotherm models for better understanding of the behaviors of silver nanoparticles adsorption onto different adsorbents," *Journal of environmental management*, vol. 218, pp. 59–70, 2018. 19

[108] N. Ayawei, A. N. Ebelegi, and D. Wankasi, "Modelling and interpretation of adsorption isotherms," *Journal of chemistry*, vol. 2017, 2017. 19

[109] M. Iwanow, T. Gärtner, V. Sieber, and B. König, "Activated carbon as catalyst support: precursors, preparation, modification and characterization," *Beilstein Journal of Organic Chemistry*, vol. 16, no. 1, pp. 1188–1202, 2020. 19

[110] İ. Demiral, C. Samdan, and H. Demiral, "Enrichment of the surface functional groups of activated carbon by modification method," *Surfaces and Interfaces*, vol. 22, p. 100873, 2021. 19

[111] A. Bhatnagar, W. Hogland, M. Marques, and M. Sillanpää, "An overview of the modification methods of activated carbon for its water treatment applications," *Chemical Engineering Journal*, vol. 219, pp. 499–511, 2013. 19

[112] X. Wang, H. Cheng, G. Ye, J. Fan, F. Yao, Y. Wang, Y. Jiao, W. Zhu, H. Huang, and D. Ye, "Key factors and primary modification methods of activated carbon and their application in adsorption of carbon-based gases: A review," *Chemosphere*, vol. 287, p. 131995, 2022. 19

[113] X. Yang, Y. Wan, Y. Zheng, F. He, Z. Yu, J. Huang, H. Wang, Y. S. Ok, Y. Jiang, and B. Gao, "Surface functional groups of carbon-based adsorbents and their roles in the removal of heavy metals from aqueous solutions: a critical review," *Chemical Engineering Journal*, vol. 366, pp. 608–621, 2019. 20

[114] J. Rivera-Utrilla, M. Sánchez-Polo, V. Gómez-Serrano, P. Álvarez, M. Alvim-Ferraz, and J. Dias, "Activated carbon modifications to enhance its water treatment applications. an overview," *Journal of hazardous materials*, vol. 187, no. 1-3, pp. 1–23, 2011. 20

[115] Y. Du, H. Chen, X. Xu, C. Wang, F. Zhou, Z. Zeng, W. Zhang, and L. Li, "Surface modification of biomass derived toluene adsorbent: hierarchically porous characterization and heteroatom doped effect," *Microporous and Mesoporous Materials*, vol. 293, p. 109831, 2020. 20

[116] M. Jeguirim, M. Belhachemi, L. Limousy, and S. Bennici, "Adsorption/reduction of nitrogen dioxide on activated carbons: textural properties versus surface chemistry–a review," *Chemical Engineering Journal*, vol. 347, pp. 493–504, 2018. 20

[117] D. Eisenberg, P. Prinsen, N. J. Geels, W. Stroek, N. Yan, B. Hua, J.-L. Luo, and G. Rothenberg, "The evolution of hierarchical porosity in self-templated nitrogen-doped carbons and its effect on oxygen reduction electrocatalysis," *RSC advances*, vol. 6, no. 84, pp. 80398–80407, 2016. 20

[118] C. Moreno-Castilla, "Adsorption of organic molecules from aqueous solutions on carbon materials," *Carbon*, vol. 42, no. 1, pp. 83–94, 2004. 21

[119] K. Foo and B. H. Hameed, "An overview of dye removal via activated carbon adsorption process," *Desalination and Water Treatment*, vol. 19, no. 1-3, pp. 255–274, 2010. 21, 45

[120] N. Soliman and A. Moustafa, "Industrial solid waste for heavy metals adsorption features and challenges; a review," *Journal of Materials Research and Technology*, vol. 9, no. 5, pp. 10235–10253, 2020. 21

[121] Z. N. Garba, W. Zhou, I. Lawan, W. Xiao, M. Zhang, L. Wang, L. Chen, and Z. Yuan, "An overview of chlorophenols as contaminants and their removal from wastewater by adsorption: A review," *Journal of environmental management*, vol. 241, pp. 59–75, 2019. 21

[122] A. Larasati, G. D. Fowler, and N. J. Graham, "Insights into chemical regeneration of activated carbon for water treatment," *Journal of Environmental Chemical Engineering*, vol. 9, no. 4, p. 105555, 2021. 21, 22

[123] A. Srivastava, B. Gupta, A. Majumder, A. K. Gupta, and S. K. Nimbhorkar, "A comprehensive review on the synthesis, performance, modifications, and regeneration of activated carbon for the adsorptive removal of various water pollutants," *Journal of Environmental Chemical Engineering*, vol. 9, no. 5, p. 106177, 2021. 21

[124] F. Salvador, N. Martin-Sanchez, R. Sanchez-Hernandez, M. J. Sanchez-Montero, and C. Izquierdo, "Regeneration of carbonaceous adsorbents. part i: thermal regeneration," *Microporous and Mesoporous Materials*, vol. 202, pp. 259–276, 2015. 22

[125] Y. Zhang, "Wet Oxidation Technology Based on Organic Wastewater Treatment," *Journal of Physics: Conference Series*, vol. 1549, no. 2, 2020. 22

[126] S. Sühnholz, F.-D. Kopinke, and B. Weiner, "Hydrothermal treatment for regeneration of activated carbon loaded with organic micropollutants," *Science of the total environment*, vol. 644, pp. 854–861, 2018. 22

[127] E. Santoso, R. Ediati, Y. Kusumawati, H. Bahruji, D. Sulistiono, and D. Prasetyoko, "Review on recent advances of carbon based adsorbent for methylene blue removal from waste water," *Materials Today Chemistry*, vol. 16, p. 100233, 2020. 22

[128] P.-J. Lu, H.-C. Lin, W.-T. Yu, and J.-M. Chern, "Chemical regeneration of activated carbon used for dye adsorption," *Journal of the Taiwan institute of chemical engineers*, vol. 42, no. 2, pp. 305–311, 2011. 22

[129] T. Alsawy, E. Rashad, M. El-Qelish, and R. H. Mohammed, "A comprehensive review on the chemical regeneration of biochar adsorbent for sustainable wastewater treatment," *Npj Clean Water*, vol. 5, no. 1, p. 29, 2022. 22

[130] M. El Gamal, H. A. Mousa, M. H. El-Naas, R. Zacharia, and S. Judd, "Bio-regeneration of activated carbon: A comprehensive review," *Separation and Purification Technology*, vol. 197, pp. 345–359, 2018. 22

[131] G. Sharma, S. Sharma, A. Kumar, C. W. Lai, M. Naushad, J. Iqbal, F. J. Stadler, *et al.*, "Activated carbon as superadsorbent and sustainable material for diverse applications," *Adsorption Science & Technology*, vol. 2022, 2022. 22

[132] J. Ani, K. Akpomie, U. Okoro, L. Aneke, O. Onukwuli, and O. Ujam, "Potentials of activated carbon produced from biomass materials for sequestration of dyes, heavy metals, and crude oil components from aqueous environment," *Applied Water Science*, vol. 10, pp. 1–11, 2020. 22

[133] T. Dutta, T. Kim, K. Vellingiri, D. C. Tsang, J. Shon, K.-H. Kim, and S. Kumar, "Recycling and regeneration of carbonaceous and porous materials through thermal or solvent treatment," *Chemical Engineering Journal*, vol. 364, pp. 514–529, 2019. 23

[134] D. Guo, Q. Shi, B. He, and X. Yuan, "Different solvents for the regeneration of the exhausted activated carbon used in the treatment of coking wastewater," *Journal of hazardous materials*, vol. 186, no. 2-3, pp. 1788–1793, 2011. 23

[135] K. G. P. Nunes, L. W. Sfreddo, M. Rosset, and L. A. Féris, "Efficiency evaluation of thermal, ultrasound and solvent techniques in activated carbon regeneration," *Environmental Technology*, vol. 42, no. 26, pp. 4189–4200, 2021. 23

[136] W. J. Weber Jr and J. C. Morris, "Kinetics of adsorption on carbon from solution," *Journal of the sanitary engineering division*, vol. 89, no. 2, pp. 31–59, 1963. 30, 47

[137] I. Temkin M, "Adsorption equilibrium and the kinetics of processes on nonhomogeneous surfaces and in the interaction between adsorbed molecules," *Zh. Fiz. Chim.*, vol. 15, pp. 296–332, 1941. 31

[138] R. Sips, "On the Structure of a Catalyst Surface," *J. Chem. Phys.*, 1948. 31

[139] Y. Liu, H. Xu, S. F. Yang, and J. H. Tay, "A general model for biosorption of Cd2+, Cu2+ and Zn2+ by aerobic granules," *Journal of Biotechnology*, vol. 102, pp. 233–239, may 2003. 31

[140] M. M. Dubinin and L. Radushkevich, "The Equation of the Characteristic Curve of Activated Charcoal," *Proceedings of the USSR Academy of Sciences*, vol. 55, pp. 327–329, 1947. 31

[141] O. Redlich and D. Peterson, "A useful adsorption isotherm," *The Journal of Chemical Physics*, vol. 63, pp. 1024–1027, 1958. 31

[142] A. N. Ebelegi, N. Ayawei, D. Wankasi, *et al.*, "Interpretation of adsorption thermodynamics and kinetics," *Open Journal of Physical Chemistry*, vol. 10, no. 03, p. 166, 2020. 31, 54

[143] D. R. Lobato-Peralta, *Carbones porosos para almacenamiento de energía*. PhD thesis, Universidad Nacional Autónoma de México, 2023. 35

[144] M. Volpe, A. Messineo, M. Mäkelä, M. R. Barr, R. Volpe, C. Corrado, and L. Fiori, "Reactivity of cellulose during hydrothermal carbonization of lignocellulosic biomass," *Fuel processing technology*, vol. 206, p. 106456, 2020. 35

[145] B. Ma, J. Zhu, B. Sun, C. Chen, and D. Sun, "Influence of pyrolysis temperature on characteristics and cr (vi) adsorption performance of carbonaceous nanofibers derived from bacterial cellulose," *Chemosphere*, vol. 291, p. 132976, 2022. 35

[146] S. Wongcharee, V. Aravinthan, L. Erdei, and W. Sanongraj, "Use of macadamia nut shell residues as magnetic nanosorbents," *International Biodeterioration & Biodegradation*, vol. 124, pp. 276–287, 2017. 38, 39, 60

[147] S. Wong, N. A. N. Yac'cob, N. Ngadi, O. Hassan, and I. M. Inuwa, "From pollutant to solution of wastewater pollution: Synthesis of activated carbon from textile sludge for dye adsorption," *Chinese Journal of Chemical Engineering*, vol. 26, no. 4, pp. 870–878, 2018. 39

[148] M. Z. U. Rehman, Z. Aslam, R. A. Shawabkeh, I. A. Hussein, and N. Mahmood, "Concurrent adsorption of cationic and anionic dyes from environmental water on amine functionalized carbon," *Water Science and Technology*, vol. 81, no. 3, pp. 466–478, 2020. 39

[149] J.-j. Gao, Y.-b. Qin, T. Zhou, D.-d. Cao, P. Xu, D. Hochstetter, and Y.-f. Wang, "Adsorption of methylene blue onto activated carbon produced from tea (camellia sinensis l.) seed shells: kinetics, equilibrium, and thermodynamics studies," *Journal of Zhejiang University Science B*, vol. 14, no. 7, pp. 650–658, 2013. 39

[150] M. Wei, F. Marrakchi, C. Yuan, X. Cheng, D. Jiang, F. F. Zafar, Y. Fu, and S. Wang, "Adsorption modeling, thermodynamics, and dft simulation of tetracycline onto mesoporous and high-surface-area naoh-activated macroalgae carbon," *Journal of Hazardous Materials*, vol. 425, p. 127887, 2022. 39

[151] J. Lang, L. Matějová, A. Cuentas-Gallegos, D. Lobato-Peralta, K. Ainassaari, M. M. Gómez, J. L. Solis, D. Mondal, R. Keiski, and G. J. Cruz, "Evaluation and selection of biochars and hydrochars derived from agricultural wastes for the use as adsorbent and energy storage materials," *Journal of Environmental Chemical Engineering*, vol. 9, no. 5, p. 105979, 2021. 39

[152] P. Larkin, *Infrared and Raman Spectroscopy: Principles and Spectral Interpretation*. Elsevier, 2011. 39

[153] A. Geethakarthi and B. Phanikumar, "Industrial sludge based adsorbents/industrial byproducts in the removal of reactive dyes–a review," *International Journal of Water Resources and Environmental Engineering*, vol. 3, no. 1, pp. 1–9, 2011. 39

[154] R. Behnam, H. Roghani-Mamaqani, and M. Salami-Kalajahi, "Preparation of carbon nanotube and polyurethane-imide hybrid composites by sol–gel reaction," *Polymer Composites*, vol. 40, no. S2, pp. E1903–E1909, 2019. 40, 58

[155] M. Thommes, K. Kaneko, A. V. Neimark, J. P. Olivier, F. Rodriguez-Reinoso, J. Rouquerol, and K. S. Sing, "Physisorption of gases, with special reference to the evaluation of surface area and pore size distribution (iupac technical report)," *Pure and applied chemistry*, vol. 87, no. 9-10, pp. 1051–1069, 2015. 41

[156] M. T. Yagub, T. K. Sen, S. Afroze, and H. M. Ang, "Dye and its removal from aqueous solution by adsorption: a review," *Advances in colloid and interface science*, vol. 209, pp. 172–184, 2014. 41

[157] D. Nayeri and S. A. Mousavi, "Dye removal from water and wastewater by nano-sized metal oxides-modified activated carbon: a review on recent researches," *Journal of Environmental Health Science and Engineering*, vol. 18, pp. 1671–1689, 2020. 42

[158] A. Kılıç and R. Orhan, "Removal of cationic dyes by adsorption in a single and binary system using activated carbon prepared from the binary mixture," *Separation Science and Technology*, vol. 54, no. 14, pp. 2147–2163, 2019. 42

[159] H. Lyu, B. Gao, F. He, A. R. Zimmerman, C. Ding, J. Tang, and J. C. Crittenden, "Experimental and modeling investigations of ball-milled biochar for the removal of aqueous methylene blue," *Chemical Engineering Journal*, vol. 335, pp. 110–119, 2018. 42

[160] Z. Esvandi, R. Foroutan, S. J. Peighambardoust, A. Akbari, and B. Ramavandi, "Uptake of anionic and cationic dyes from water using natural clay and clay/starch/mnfe2o4 magnetic nanocomposite," *Surfaces and Interfaces*, vol. 21, p. 100754, 2020. 42

[161] R. J. Martínez, A. Z. Vela-Carrillo, L. A. Godínez, J. de Jesús Pérez-Bueno, and I. Robles, "Competitive adsorption of anionic and cationic molecules on three activated carbons derived from agroindustrial waste," *Biomass and Bioenergy*, vol. 168, p. 106660, 2023. 42

[162] V. Homem, A. Alves, and L. Santos, "Amoxicillin removal from aqueous matrices by sorption with almond shell ashes," *International journal of environmental and analytical chemistry*, vol. 90, no. 14-15, pp. 1063–1084, 2010. 43

[163] J. Imanipoor, M. Mohammadi, M. Dinari, and M. R. Ehsani, "Adsorption and desorption of amoxicillin antibiotic from water matrices using an effective and recyclable mil-53 (al) metal–organic framework adsorbent," *Journal of Chemical & Engineering Data*, vol. 66, no. 1, pp. 389–403, 2020. 43

[164] M. E. Fernandez, G. V. Nunell, P. R. Bonelli, and A. L. Cukierman, "Activated carbon developed from orange peels: Batch and dynamic competitive adsorption of basic dyes," *Industrial crops and products*, vol. 62, pp. 437–445, 2014. 44

[165] C. Pelekani and V. L. Snoeyink, "Competitive adsorption between atrazine and methylene blue on activated carbon: the importance of pore size distribution," *Carbon*, vol. 38, no. 10, pp. 1423–1436, 2000. 44

[166] C.-T. Hsieh and H. Teng, "Influence of mesopore volume and adsorbate size on adsorption capacities of activated carbons in aqueous solutions," *Carbon*, vol. 38, no. 6, pp. 863–869, 2000. 44

[167] G. L. Dotto and L. A. d. A. Pinto, "Analysis of mass transfer kinetics in the biosorption of synthetic dyes onto spirulina platensis nanoparticles," *Biochemical Engineering Journal*, vol. 68, pp. 85–90, 2012. 47

[168] G. F. Malash and M. I. El-Khaiary, "Piecewise linear regression: A statistical method for the analysis of experimental adsorption data by the intraparticle-diffusion models," *Chemical Engineering Journal*, vol. 163, no. 3, pp. 256–263, 2010. 47

[169] G. L. Dotto, J. A. V. Costa, and L. A. d. A. Pinto, "Kinetic studies on the biosorption of phenol by nanoparticles from spirulina sp. leb 18," *Journal of Environmental Chemical Engineering*, vol. 1, no. 4, pp. 1137–1143, 2013. 47

[170] F. Chen, W. Liang, X. Qin, L. Jiang, Y. Zhang, S. Fang, and D. Luo, "Preparation and recycled simultaneous adsorption of methylene blue and cu2+ co-pollutants over carbon layer encapsulated fe3o4/graphene oxide nanocomposites rich in amino and thiol groups," *Colloids and Surfaces A: Physicochemical and Engineering Aspects*, vol. 625, p. 126913, 2021. 48

[171] F.-C. Wu, R.-L. Tseng, and R.-S. Juang, "Initial behavior of intraparticle diffusion model used in the description of adsorption kinetics," *Chemical engineering journal*, vol. 153, no. 1-3, pp. 1–8, 2009. 48, 49

[172] K. M. Doke and E. M. Khan, "Adsorption thermodynamics to clean up wastewater; critical review," *Reviews in Environmental Science and Bio/Technology*, vol. 12, no. 1, pp. 25–44, 2013. 54

[173] V. J. Inglezakis and A. A. Zorpas, "Heat of adsorption, adsorption energy and activation energy in adsorption and ion exchange systems," *Desalination and water treatment*, vol. 39, no. 1-3, pp. 149–157, 2012. 54

[174] E. Caldin and G. Long, "The equilibrium between ethoxide and hydroxide ions in ethanol and in ethanol–water mixtures," *Journal of the Chemical Society (Resumed)*, pp. 3737–3742, 1954. 56

[175] A. Larasati, G. D. Fowler, and N. J. Graham, "Chemical regeneration of granular activated carbon: preliminary evaluation of alternative regenerant solutions," *Environmental Science: Water Research & Technology*, vol. 6, no. 8, pp. 2043–2056, 2020. 56

[176] J. Zhang, Y. P. Chen, K. P. Miller, M. S. Ganewatta, M. Bam, Y. Yan, M. Nagarkatti, A. W. Decho, and C. Tang, "Antimicrobial metallopolymers and their bioconjugates with conventional antibiotics against multidrug-resistant bacteria," *Journal of the American Chemical Society*, vol. 136, no. 13, pp. 4873–4876, 2014. 56

[177] J. Zhang, J. Yan, P. Pageni, Y. Yan, A. Wirth, Y.-P. Chen, Y. Qiao, Q. Wang, A. W. Decho, and C. Tang, "Anion-responsive metallopolymer hydrogels for healthcare applications," *Scientific reports*, vol. 5, no. 1, pp. 1–10, 2015. 56

[178] A. Ahmad and B. Hameed, "Reduction of cod and color of dyeing effluent from a cotton textile mill by adsorption onto bamboo-based activated carbon," *Journal of hazardous materials*, vol. 172, no. 2-3, pp. 1538–1543, 2009. 58

[179] K. Nath, S. Panchani, M. Bhakhar, and S. Chatrola, "Preparation of activated carbon from dried pods of prosopis cineraria with zinc chloride activation for the removal of phenol," *Environmental Science and Pollution Research*, vol. 20, pp. 4030–4045, 2013. 58

[180] I. Sulistianti, Y. Krisnandi, and I. Moenandar, "Study of co2 adsorption capacity of mesoporous carbon and activated carbon modified by triethylenetetramine (teta)," in *IOP Conference Series: Materials Science and Engineering*, vol. 188, p. 012041, IOP Publishing, 2017. 58

[181] X. D. Dai, X. M. Liu, G. Zhao, L. Qian, K. Qiao, and Z. F. Yan, "Treatment of activated carbon for methane storage," *Asia-Pacific Journal of Chemical Engineering*, vol. 3, no. 3, pp. 292–297, 2008. 58

[182] A. M. Vargas, A. L. Cazetta, M. H. Kunita, T. L. Silva, and V. C. Almeida, "Adsorption of methylene blue on activated carbon produced from flamboyant pods (delonix regia): Study of adsorption isotherms and kinetic models," *Chemical Engineering Journal*, vol. 168, no. 2, pp. 722–730, 2011. 58

[183] Y. Xie, "Electrochemical performance of polyaniline support on electrochemical activated carbon fiber," *Journal of Materials Engineering and Performance*, vol. 31, no. 3, pp. 1949–1955, 2022. 58

[184] M. Asadullah, M. Asaduzzaman, M. S. Kabir, M. G. Mostofa, and T. Miyazawa, "Chemical and structural evaluation of activated carbon prepared from jute sticks for brilliant green dye removal from aqueous solution," *Journal of hazardous materials*, vol. 174, no. 1-3, pp. 437–443, 2010. 58

[185] S. Ge, Z. Liu, R. Li, Y. Furuta, and W. Peng, "Desulphurization characteristics of bamboo charcoal from sulfur solution," *Saudi Journal of Biological Sciences*, vol. 24, no. 1, pp. 127–131, 2017. 58

[186] S. Wongcharee and V. Aravinthan, "Application of mesoporous magnetic nanosorbent developed from macadamia nut shell residues for the removal of recalcitrant melanoidin and its fractions," *Separation Science and Technology*, vol. 55, no. 9, pp. 1636–1649, 2020. 60

[187] S. Wongcharee, V. Aravinthan, and L. Erdei, "Mesoporous activated carbon-zeolite composite prepared from waste macadamia nut shell and synthetic faujasite," *Chinese journal of chemical engineering*, vol. 27, no. 1, pp. 226–236, 2019. 60

[188] C. Du, Y. Xue, Z. Wu, and Z. Wu, "Microwave-assisted one-step preparation of macadamia nut shell-based activated carbon for efficient adsorption of reactive blue," *New Journal of Chemistry*, vol. 41, no. 24, pp. 15373–15383, 2017. 60

[189] Y. Jiang, J. Ye, Q. Feng, W. Yang, *et al.*, "Exploration and optimization for methylene blue dye removal with modified macadamia nut shell.," *Desalination and Water Treatment*, vol. 95, pp. 295–307, 2017. 60